Nonlocal and localized analyses of conditional mean transient flow in bounded, randomly heterogeneous porous media

Ming Ye[1] and Shlomo P. Neuman
Department of Hydrology and Water Resources, University of Arizona, Tucson, Arizona, USA

Alberto Guadagnini
Dipartimento di Ingegneria Idraulica Ambientale e del Rilevamento, Politecnico di Milano, Milan, Italy

Daniel M. Tartakovsky
Theoretical Division, Los Alamos National Laboratory, Los Alamos, New Mexico, USA

Received 25 February 2003; revised 10 February 2004; accepted 17 February 2004; published 12 May 2004.

[1] We consider the numerical prediction of transient flow in bounded, randomly heterogeneous porous media driven by random sources, initial heads, and boundary conditions without resorting to Monte Carlo simulation. After applying the Laplace transform to the governing stochastic flow equations, we derive exact nonlocal (integro-differential) equations for the mean and variance-covariance of transformed head and flux, conditioned on measured values of log conductivity $Y = \ln K$. Approximating these conditional moment equations recursively to second order in the standard deviation σ_Y of Y, we solve them by finite elements for superimposed mean-uniform and convergent flows in a two-dimensional domain. An alternative conditional mean solution is obtained through localization of the exact moment expressions. The nonlocal and localized solutions are obtained using a highly efficient parallel algorithm and inverted numerically back into the time domain. A comparison with Monte Carlo simulations demonstrates that the moment solutions are remarkably accurate for strongly heterogeneous media with σ_Y^2 as large as 4. The nonlocal solution is only slightly more accurate than the much simpler localized solution, but the latter does not yield information about predictive uncertainty. The accuracy of each solution improves markedly with conditioning. A preliminary comparison of computational efficiency suggests that both the nonlocal and localized solutions for mean head and its variance require significantly less computer time than is required for Monte Carlo statistics to stabilize when the same direct matrix solver is used for all three (we do not presently know how using iterative solvers would have affected this conclusion). This is true whether the Laplace inversion and Monte Carlo simulations are conducted sequentially or in parallel on multiple processors and regardless of problem size. The underlying exact and recursive moment equations, as well as the proposed computational algorithm, are valid in both two and three dimensions; only the numerical implementation of our algorithm is two-dimensional. *INDEX TERMS:* 1829 Hydrology: Groundwater hydrology; 1869 Hydrology: Stochastic processes; 3210 Mathematical Geophysics: Modeling; 3230 Mathematical Geophysics: Numerical solutions; *KEYWORDS:* transient flow, uncertainty, heterogeneity, spatial variability, localization, parallel computing

Citation: Ye, M., S. P. Neuman, A. Guadagnini, and D. M. Tartakovsky (2004), Nonlocal and localized analyses of conditional mean transient flow in bounded, randomly heterogeneous porous media, *Water Resour. Res.*, *40*, W05104, doi:10.1029/2003WR002099.

1. Introduction

[2] Hydraulic parameters vary randomly in space and are therefore often modeled as spatially correlated random fields. This, together with uncertainty in forcing terms (initial conditions, boundary conditions and sources), renders the groundwater flow equations stochastic. The solution of such equations consists of the joint, multivariate probability distribution of its dependent variables or, equivalently, the corresponding ensemble moments. It is advantageous to condition the solution on measured values of input variables (parameters and forcing terms) at discrete point in space-time (conditioning on measured values of the dependent variables requires an inverse solution and is not discussed here). The equations can then be solved by conditional Monte Carlo simulation or by approximation. A typical solution includes the first two

[1] Now at Pacific Northwest National Laboratory, Richland, Washington, USA.

0043-1397/04/2003WR002099$09.00

conditional moments (mean and variance-covariance) of head and flux. The first moments constitute optimum unbiased predictors of these random quantities, and the second moments are measures of the associated prediction errors.

[3] The Monte Carlo approach is conceptually straightforward but requires knowing or assuming the joint multivariate distribution of all random inputs parameters and forcing terms; is computationally demanding; and lacks theoretical convergence criteria for moments higher than the mean (for which such criteria exist, e.g., *Morgan and Henrion* [1990] and *Shapiro and Homem-de-mello* [2000]). Its computational burden stems from the need to (1) generate random realizations of the input parameters (e.g., log-conductivity) on a grid that is much finer than their spatial correlation (integral) scale, so as to preserve their geostatistical properties; (2) solve the flow problem numerically on this fine grid; (3) repeat steps 1 and 2 many times (typically thousands) for a given set of random forcing functions, so as to minimize sampling error; and (4) repeat steps $1-3$ for each set of random forcing functions representing different scenarios.

[4] We focus on an alternative that allows computing leading conditional ensemble moments of head and flux directly by solving a recursive system of moment equations. The moment equations are distribution free and thus obviate the need to know or assume the multivariate distributions of random input parameters or forcing terms. *Tartakovsky and Neuman* [1998a] developed exact integro-differential equations for the first two conditional moments of head and flux in a bounded, randomly heterogeneous domain. Their equations are nonlocal and non-Darcian in that the mean flux depends on mean head gradients at more than one point in space-time. *Tartakovsky and Neuman* [1998b] explored ways to localize the exact conditional mean equations in real, Laplace- and/or infinite Fourier-transformed domains so as to render them Darcian. Such localization entails an approximation which does not extend to moments higher than one. To render the nonlocal moment equations workable, *Tartakovsky and Neuman* [1998a] approximated them recursively through expansion in powers of σ_Y, a measure of the conditional standard deviation of log conductivity $Y = \ln K$. Their recursive approximations are nominally limited either to mildly heterogeneous $\sigma_Y \leq 1$ or to well-conditioned strongly heterogeneous media $\sigma_Y > 1$. The authors have not evaluated their expressions numerically.

[5] In this paper we develop analogous recursive approximations in Laplace space and solve them by a finite element algorithm patterned after that developed for steady state flow by *Guadagnini and Neuman* [1999a, 1999b]. The moment equations include Green's functions that need to be computed once for a given boundary configuration and are then applicable to a variety of forcing scenarios. For comparison, we compute conditional mean head and flux by finite elements in Laplace space using (1) a localized version of the exact moment equations and (2) a standard Monte Carlo approach. We do so for superimposed mean-uniform and convergent flows in a two-dimensional domain. All three sets of solutions are inverted numerically back into the time domain by using a parallelized version of an algorithm due to *Crump* [1976] and *De Hoog et al.* [1982]. Previously, sequential or parallel versions of this algorithm were used to solve deterministic flow and transport problems by *Sudicky* [1989], *Xu and Brusseau* [1995], *Gambolati et al.* [1997], *Pini and Putti* [1997], and *Farrell et al.* [1998], and to conduct Monte Carlo simulations of transport by *Naff et al.* [1998]. We assess the relative accuracies of the recursive nonlocal and localized solutions through comparison with the Monte Carlo results. We compare the computational efficiencies of unconditional recursive nonlocal and Monte Carlo solutions as functions of grid size for the special case where a single direct matrix solver is applied to both. A more comprehensive comparison of computational efficiencies, in which recursive nonlocal moment and Monte Carlo solutions are obtained in manners that are optimal for each, is outside the scope of this study.

[6] Our approach differs from standard perturbative solutions [e.g., *Dagan*, 1982; *Indelman*, 1996, 2000, 2002; *Zhang*, 1999, 2002] in several ways. On a fundamental level, our approach originates in a set of conditional moment equations that are exact, compact, formally incorporate boundary effects, provide a unique insight into the nature of the problem (as explained by *Neuman* [1997, 2002]), and lead to unique localized moment equations that look like standard deterministic flow (and transport) equations, allowing one to interpret the latter within a conditional stochastic framework [*Neuman and Guadagnini*, 2000; *Guadagnini and Neuman*, 2001]. Both the nonlocal and localized equations describe the spatial-time evolution of moments representing random functions rendered statistically inhomogeneous (in space) and nonstationary (in time) due to the combined effects of sources, boundaries, and conditioning. To approximate the exact moment equations recursively, we use a valid expansion in terms of (deterministic) moments rather than a theoretically invalid expansion in terms of random quantities [e.g., *Dagan*, 1989; *Zhang*, 2002], which may (but is not guaranteed) to yield valid results after subsequent averaging.

[7] On a practical level, our approach leads to localized moment equations that are almost as easy to solve as standard deterministic flow equations, and to recursive nonlocal moment equations written in terms of Green's functions, which are independent of internal sources and the magnitudes of boundary terms. Once these functions have been computed for a given boundary configuration, they can be used repeatedly to obtain solutions for a wide range of internal sources and boundary terms (scenarios). The same is not true for standard perturbation expressions such as those developed for transient flow in bounded domains by *Zhang* [1999].

[8] The underlying exact and recursive moment equations, as well as the proposed computational algorithm, are valid in both two and three dimensions, though we implement them numerically in two dimensions.

2. Statement of Problem

[9] We consider transient flow in a domain Ω governed by Darcy's law

$$\mathbf{q}(\mathbf{x}, t) = -K(\mathbf{x})\nabla h(\mathbf{x}, t) \qquad \mathbf{x} \in \Omega \tag{1}$$

and the continuity equation

$$S_s(\mathbf{x})\frac{\partial h}{\partial t} = -\nabla \cdot \mathbf{q}(\mathbf{x},t) + f(\mathbf{x},t) \qquad \mathbf{x} \in \Omega \tag{2}$$

subject to initial and boundary conditions

$$h(\mathbf{x},0) = H_0(\mathbf{x}) \qquad \mathbf{x} \in \Omega \tag{3}$$

$$h(\mathbf{x},t) = H(\mathbf{x},t) \qquad \mathbf{x} \in \Gamma_D \tag{4}$$

$$-\mathbf{q}(\mathbf{x},t)\cdot\mathbf{n}(\mathbf{x}) = Q(\mathbf{x},t) \qquad \mathbf{x} \in \Gamma_N \tag{5}$$

where $\mathbf{q}$ is Darcy flux, $\mathbf{x}$ is a vector of space coordinates, t is time, K is a scalar hydraulic conductivity forming a correlated random field, h is hydraulic head, S_s is a deterministic specific storage term, f is a random source term, $H_0(\mathbf{x})$ is random initial head, H is randomly prescribed head on Dirichlet boundaries Γ_D, Q is random flux into the flow domain across Neumann boundaries Γ_N, and $\mathbf{n}$ is a unit vector normal to the boundary $\Gamma = \Gamma_D \cup \Gamma_N$ pointing out of the domain. The forcing terms f, H_0, H, and Q are taken to be uncorrelated with each other or with K.

[10] All quantities in equations (1)–(5) are defined on a consistent nonzero support volume ω, centered around $\mathbf{x}$, which is small in comparison to Ω but sufficiently large for Darcy's law to be locally valid [*Neuman and Orr*, 1993]. This operational definition of ω does not generally conform to a representative elementary volume (REV) in the traditional sense [*Bear*, 1972]. Conditioning and the action of forcing terms render the solution of equations (1)–(5) nonstationary in space-time.

[11] The Laplace transform of a function $g(t)$ is defined as [*Carslaw and Jaeger*, 1959]

$$\mathcal{L}[g(t)] = \overline{g}(\lambda) = \int_0^\infty g(t)e^{-\lambda t}dt \tag{6}$$

where λ is a complex Laplace parameter. The Laplace transform of a derivative is

$$\mathcal{L}\left[\frac{dg}{dt}\right] = \lambda\overline{g}(\lambda) - g(0) \tag{7}$$

Applying equations (6) and (7) to (1)–(5) yields transformed flow equations

$$\overline{\mathbf{q}}(\mathbf{x},\lambda) = -K(\mathbf{x})\nabla\overline{h}(\mathbf{x},\lambda) \qquad \mathbf{x} \in \Omega \tag{8}$$

$$\nabla\cdot\overline{\mathbf{q}}(\mathbf{x},\lambda) + S_s(\mathbf{x})\lambda\overline{h}(\mathbf{x},\lambda) = \overline{f}(\mathbf{x},\lambda) + S_s(\mathbf{x})H_0(\mathbf{x}) \qquad \mathbf{x} \in \Omega \tag{9}$$

$$\overline{h}(\mathbf{x},\lambda) = \overline{H}(\mathbf{x},\lambda) \qquad \mathbf{x} \in \Gamma_D \tag{10}$$

$$-\overline{\mathbf{q}}(\mathbf{x},\lambda)\cdot\mathbf{n}(\mathbf{x}) = \overline{Q}(\mathbf{x},\lambda) \qquad \mathbf{x} \in \Gamma_N \tag{11}$$

where $\overline{H}$, $\overline{\mathbf{q}}$, $\overline{H}$, $\overline{Q}$, and $\overline{f}$ are Laplace transforms of h, $\mathbf{q}$, H, Q, and f, respectively.

3. Exact Conditional Moment Equations

[12] Let $\langle K(\mathbf{x})\rangle_c$ be the ensemble mean of $K(\mathbf{x})$ conditioned on ω-scale measurements at a set of discrete points in Ω. As such, $\langle K(\mathbf{x})\rangle_c$ forms a relatively smooth optimum unbiased estimate of the fluctuating random function $K(\mathbf{x})$. The unknown hydraulic conductivity $K(\mathbf{x})$ differs from its known estimate $\langle K(\mathbf{x})\rangle_c$ by a zero mean random estimation error $K'(\mathbf{x})$ such that

$$K(\mathbf{x}) = \langle K(\mathbf{x})\rangle_c + K'(\mathbf{x}) \qquad \langle K'(\mathbf{x})\rangle_c = 0 \tag{12}$$

Likewise we write

$$\overline{h}(\mathbf{x},\lambda) = \langle\overline{h}(\mathbf{x},\lambda)\rangle_c + \overline{h'}(\mathbf{x},\lambda)\left\langle\overline{h'}(\mathbf{x},\lambda)\right\rangle_c = 0 \tag{13}$$

$$\overline{\mathbf{q}}(\mathbf{x},\lambda) = \langle\overline{\mathbf{q}}(\mathbf{x},\lambda)\rangle_c + \overline{\mathbf{q}'}(\mathbf{x},\lambda)\langle\overline{\mathbf{q}'}(\mathbf{x},\lambda)\rangle_c = 0 \tag{14}$$

3.1. Exact Conditional Mean Equations

[13] Substituting equations (12)–(14) into (8)–(11) and taking conditional ensemble mean yields the following exact conditional mean equations for the Laplace transform of head:

$$\begin{aligned}\langle\overline{\mathbf{q}}(\mathbf{x},\lambda)\rangle_c &= -\langle K(\mathbf{x})\rangle_c\nabla\left\langle\overline{h}(\mathbf{x},\lambda)\right\rangle_c + \overline{\mathbf{r}}_c(\mathbf{x},\lambda)\\ \overline{\mathbf{r}}_c(\mathbf{x},\lambda) &= -\left\langle K'(\mathbf{x})\nabla\overline{h}'(\mathbf{x},\lambda)\right\rangle_c \qquad \mathbf{x}\in\Omega\end{aligned} \tag{15}$$

$$\begin{aligned}&\nabla\cdot\langle\overline{\mathbf{q}}(\mathbf{x},\lambda)\rangle_c + S_s(\mathbf{x})\lambda\left\langle\overline{h}(\mathbf{x},\lambda)\right\rangle_c\\ &\quad= \left\langle\overline{f}(\mathbf{x},\lambda)\right\rangle + S_s(\mathbf{x})\langle H_0(\mathbf{x})\rangle \qquad \mathbf{x}\in\Omega\end{aligned} \tag{16}$$

$$\left\langle\overline{h}(\mathbf{x},\lambda)\right\rangle_c = \left\langle\overline{H}(\mathbf{x},\lambda)\right\rangle \qquad \mathbf{x}\in\Gamma_D \tag{17}$$

$$-\langle\overline{\mathbf{q}}(\mathbf{x},\lambda)\rangle_c\cdot\mathbf{n}(\mathbf{x}) = \left\langle\overline{Q}(\mathbf{x},\lambda)\right\rangle \qquad \mathbf{x}\in\Gamma_N \tag{18}$$

where $\langle\overline{f}\rangle$, $\langle H_0\rangle$, $\langle\overline{H}\rangle$, and $\langle\overline{Q}\rangle$ are unconditional ensemble mean forcing terms and $\overline{\mathbf{r}}$ is a transformed "residual flux." As shown in Appendix A, the latter is given implicitly by

$$\overline{\mathbf{r}}_c(\mathbf{x},\lambda) = \int_\Omega \overline{\mathbf{a}}_c(\mathbf{y},\mathbf{x},\lambda)\nabla_{\mathbf{y}}\left\langle\overline{h}(\mathbf{y},\lambda)\right\rangle_c d\mathbf{y} + \int_\Omega \overline{\mathbf{d}}_c(\mathbf{y},\mathbf{x},\lambda)\overline{\mathbf{r}}_c(\mathbf{y},\lambda)d\mathbf{y} \tag{19}$$

with kernels

$$\overline{\mathbf{a}}_c(\mathbf{y},\mathbf{x},\lambda) = \left\langle K'(\mathbf{x})K'(\mathbf{y})\nabla_{\mathbf{x}}\nabla_{\mathbf{y}}^T\overline{G}(\mathbf{y},\mathbf{x},\lambda)\right\rangle_c \tag{20}$$

$$\overline{\mathbf{d}}_c(\mathbf{y},\mathbf{x},\lambda) = \left\langle K'(\mathbf{x})\nabla_{\mathbf{x}}\nabla_{\mathbf{y}}^T\overline{G}(\mathbf{y},\mathbf{x},\lambda)\right\rangle_c \tag{21}$$

Here $\overline{G}(\mathbf{y}, \mathbf{x}, \lambda)$ is a transformed random Green's function defined in Appendix A. The kernels are similar to those obtained for steady state [*Guadagnini and Neuman*, 1999a] except that they include the complex Laplace parameter λ. From equations (15) and (19) it is evident that the transformed residual and mean flux are nonlocal in space (they depend on mean head gradient at points other than $\mathbf{x}$) and non-Darcian (there is no effective or equivalent hydraulic conductivity valid for arbitrary directions of conditional mean flow in Laplace space).

3.2. Exact Conditional Second Moment Equations

[14] Let $C_{hc}(\mathbf{x}, \mathbf{y}, t, s) = \langle h'(\mathbf{x}, t)h'(\mathbf{y}, s)\rangle_c$ be the conditional covariance of head corresponding to two points $(\mathbf{x}, t)$ and $(\mathbf{y}, s)$ in space-time. Applying Laplace transform to $C_{hc}(\mathbf{x}, \mathbf{y}, t, s)$ with respect to t yields a transformed conditional covariance $\overline{C}_{hc}(\mathbf{x}, \underline{\mathbf{y}}, \lambda, s) = \langle \overline{h'}(\mathbf{x}, \lambda)h'(\mathbf{y}, s)\rangle_c$ between the transformed head $\overline{h}(\mathbf{x}, \lambda)$ and the original head $h(\mathbf{y}, s)$. Similarly, $\overline{\mathbf{C}}_{\mathbf{q}c}(\mathbf{x}, \mathbf{y}, \lambda, s) = \langle \overline{\mathbf{q}'}(\mathbf{x}, \lambda)\overline{\mathbf{q}}'^{T}(\mathbf{y}, s)\rangle_c$ is a transformed conditional cross-covariance tensor between the transformed flux $\overline{\mathbf{q}}(\mathbf{x}, \lambda)$ and the original flux $\mathbf{q}(\mathbf{y}, s)$, the superscript T denoting transpose.

[15] We show in Appendix B that $\overline{C}_{hc}(\mathbf{x}, \mathbf{y}, \lambda, s)$ satisfies exactly the equation

$$
\begin{aligned}
&-\nabla_{\mathbf{x}} \cdot \Big[\langle K(\mathbf{x})\rangle_c \nabla_{\mathbf{x}} \overline{C}_{hc}(\mathbf{x}, \mathbf{y}, \lambda, s) + \overline{\mathbf{P}}_c(\mathbf{x}, \mathbf{y}, \lambda, s) \\
&+ u_c(\mathbf{x}, \mathbf{y}, s)\nabla_{\mathbf{x}}\langle \overline{h}(\mathbf{x}, \lambda)\rangle_c\Big] + S_s(\mathbf{x})\lambda \overline{C}_{hc}(\mathbf{x}, \mathbf{y}, \lambda, s) \\
&= S_s(\mathbf{x})\langle H_0'(\mathbf{x})h'(\mathbf{y}, s)\rangle_c + \left\langle \overline{f}'(\mathbf{x}, \lambda)h'(\mathbf{y}, s)\right\rangle_c \qquad \mathbf{x} \in \Omega
\end{aligned} \tag{22}
$$

subject to boundary conditions

$$
\overline{C}_{hc}(\mathbf{x}, \mathbf{y}, \lambda, s) = \left\langle \overline{H}'(\mathbf{x}, \lambda)h'(\mathbf{y}, s)\right\rangle_c \quad \mathbf{x} \in \Gamma_D \tag{23}
$$

$$
\begin{aligned}
&\Big[\langle K(\mathbf{x})\rangle_c \nabla_{\mathbf{x}} \overline{C}_{hc}(\mathbf{x}, \mathbf{y}, \lambda, s) + \overline{\mathbf{P}}_c(\mathbf{x}, \mathbf{y}, \lambda, s) + u_c(\mathbf{x}, \mathbf{y}, s) \\
&\cdot \nabla_{\mathbf{x}}\langle \overline{h}(\mathbf{x}, \lambda)\rangle_c\Big] \cdot \mathbf{n}(\mathbf{x}) = \left\langle \overline{Q}'(\mathbf{x}, \lambda)h'(\mathbf{y}, s)\right\rangle_c \qquad \mathbf{x} \in \Gamma_N
\end{aligned} \tag{24}
$$

where $\overline{\mathbf{P}}_c(\mathbf{x}, \mathbf{y}, \lambda, s) = \langle K'(\mathbf{x})\nabla_{\mathbf{x}}\overline{h}'(\mathbf{x}, \lambda)h'(\mathbf{y}, s)\rangle_c$ is a third moment given explicitly by

$$
\begin{aligned}
&\overline{\mathbf{P}}_c(\mathbf{x}, \mathbf{y}, \lambda, s) = \\
&-\int_0^s \int_\Omega \nabla_{\mathbf{z}}\left\langle K'(\mathbf{x})\nabla_{\mathbf{x}}\overline{h}'(\mathbf{x}, \lambda)\nabla_{\mathbf{z}}^T G(\mathbf{z}, \mathbf{y}, s-\tau)\right\rangle_c \mathbf{r}_c(\mathbf{z}, \tau)d\mathbf{z}d\tau \\
&-\int_0^s \int_\Omega \left\langle K'(\mathbf{x})K'(\mathbf{z})\nabla_{\mathbf{x}}\overline{h}'(\mathbf{x}, \lambda)\nabla_{\mathbf{z}}^T G(\mathbf{z}, \mathbf{y}, s-\tau)\right\rangle_c \\
&\quad \times \nabla_{\mathbf{z}}\langle h(\mathbf{z}, \tau)\rangle_c d\mathbf{z}d\tau \\
&+\int_\Omega S_s(\mathbf{z})\left\langle H_0'(\mathbf{z})G(\mathbf{z}, \mathbf{y}, s)K'(\mathbf{x})\nabla_{\mathbf{x}}\overline{h}'(\mathbf{x}, \lambda)\right\rangle_c d\mathbf{z} \\
&+\int_0^s \int_\Omega \left\langle f'(\mathbf{z}, \tau)G(\mathbf{z}, \mathbf{y}, s-\tau)K'(\mathbf{x})\nabla_{\mathbf{x}}\overline{h}'(\mathbf{x}, \lambda)\right\rangle_c d\mathbf{z}d\tau \\
&-\int_0^s \int_{\Gamma_D} \langle K'(\mathbf{x})K(\mathbf{z})H'(\mathbf{z}, \tau)\nabla_{\mathbf{x}}\overline{h}'(\mathbf{x}, \lambda)\nabla_{\mathbf{z}}^T G(\mathbf{z}, \mathbf{y}, s-\tau)\rangle_c \\
&\quad \cdot \mathbf{n}(\mathbf{z})d\mathbf{z}d\tau \\
&+\int_0^s \int_{\Gamma_N} \left\langle Q'(\mathbf{z}, \tau)K'(\mathbf{x}).G(\mathbf{z}, \mathbf{y}, s-\tau)\nabla_{\mathbf{x}}\overline{h}'(\mathbf{x}, \lambda)\right\rangle_c d\mathbf{z}d\tau
\end{aligned} \tag{25}
$$

The conditional cross covariance $u_c(\mathbf{x}, \mathbf{y}, s) = \langle K'(\mathbf{x})h'(\mathbf{y}, s)\rangle_c$ between head and conductivity is given by

$$
\begin{aligned}
&u_c(\mathbf{x}, \mathbf{y}, s) = \\
&-\int_0^s \int_\Omega \mathbf{r}_c(\mathbf{z}, \tau) \cdot \nabla_{\mathbf{z}} \cdot \langle G(\mathbf{z}, \mathbf{y}, s-\tau)K'(\mathbf{x})\rangle_c d\mathbf{z}d\tau \\
&-\int_0^s \int_\Omega \nabla_{\mathbf{z}}\langle h(\mathbf{z}, \tau)\rangle_c \cdot \langle K'(\mathbf{z})\nabla_{\mathbf{z}}G(\mathbf{z}, \mathbf{y}, s-\tau)K'(\mathbf{x})\rangle_c d\mathbf{z}d\tau
\end{aligned} \tag{26}
$$

as in equation (53) of *Tartakovsky and Neuman* [1998a]. Explicit expressions for $\langle H_0'h'\rangle_c$, $\langle \bar{f}'h'\rangle_c$, $\langle \bar{H}'h'\rangle_c$, and $\langle \bar{Q}'h'\rangle_c$ are given in Appendix B. The conditional head variance $C_{hc}(\mathbf{x}, \underline{\mathbf{x}}, t, t)$ can be obtained through inverse transformation of $\overline{C}_{hc}(\mathbf{x}, \mathbf{x}, \lambda, t)$ at time t. The latter is given explicitly by (Appendix B)

$$
\begin{aligned}
&\overline{C}_{hc}(\mathbf{x}, \mathbf{x}, \lambda, t) = \left\langle \bar{h}'(\mathbf{x}, \lambda)h'(\mathbf{x}, t)\right\rangle_c = \\
&\int_\Omega \left\langle K'(\mathbf{y})\nabla\bar{h}'(\mathbf{y}, \lambda)\right\rangle_c \cdot \langle \nabla_{\mathbf{y}}\overline{G}(\mathbf{y}, \mathbf{x}, \lambda)h'(\mathbf{x}, t)\rangle_c d\mathbf{y} \\
&-\int_\Omega \nabla\langle \bar{h}(\mathbf{y}, \lambda)\rangle_c \cdot \langle K'(\mathbf{y})\nabla_{\mathbf{y}}\overline{G}(\mathbf{y}, \mathbf{x}, \lambda)h'(\mathbf{x}, t)\rangle_c d\mathbf{y} \\
&+\int_\Omega \left\langle \bar{f}'(\mathbf{y}, \lambda)\overline{G}(\mathbf{y}, \mathbf{x}, \lambda)h'(\mathbf{x}, t)\right\rangle_c d\mathbf{y} \\
&+\int_\Omega S_s(\mathbf{y})\langle H_0'(\mathbf{y})\overline{G}(\mathbf{y}, \mathbf{x}, \lambda)h'(\mathbf{x}, t)\rangle_c d\mathbf{y} \\
&-\int_{\Gamma_D} \left\langle \bar{H}'(\mathbf{y}, \lambda)K(\mathbf{y})\nabla_{\mathbf{y}}\overline{G}(\mathbf{y}, \mathbf{x}, \lambda)h'(\mathbf{x}, t)\right\rangle_c \cdot \mathbf{n}(\mathbf{y})d\mathbf{y} \\
&+\int_{\Gamma_N} \left\langle \bar{Q}'(\mathbf{y}, \lambda)\overline{G}(\mathbf{y}, \mathbf{x}, \lambda)h'(\mathbf{x}, t)\right\rangle_c d\mathbf{y}
\end{aligned} \tag{27}
$$

[16] The conditional cross-covariance tensor $\overline{\mathbf{C}}_{\mathbf{q}c}(\mathbf{x}, \mathbf{y}, \lambda, s) = \langle \overline{\mathbf{q}}'(\mathbf{x}, \lambda)\mathbf{q}'^{T}(\mathbf{y}, s)\rangle_c$ of the flux is given explicitly by (Appendix B)

$$
\begin{aligned}
&\overline{\mathbf{C}}_{\mathbf{q}c}(\mathbf{x}, \mathbf{y}, \lambda, s) = -\overline{\mathbf{r}}_c(\mathbf{x}, \lambda)\mathbf{r}_c^T(\mathbf{y}, s) \\
&+\langle K(\mathbf{x})\rangle_c \nabla_{\mathbf{x}}\nabla_{\mathbf{y}}^T \overline{C}_{hc}(\mathbf{x}, \mathbf{y}, \lambda, s)\langle K(\mathbf{y})\rangle_c \\
&+\langle K(\mathbf{x})\rangle_c \nabla_{\mathbf{x}}\overline{u}_c(\mathbf{y}, \mathbf{x}, \lambda)\nabla_{\mathbf{y}}^T\langle h(\mathbf{y}, s)\rangle_c \\
&+\langle K(\mathbf{x})\rangle_c \left\langle K'(\mathbf{y})\nabla_{\mathbf{x}}\overline{h}'(\mathbf{x}, \lambda)\nabla_{\mathbf{y}}^T h'(\mathbf{y}, s)\right\rangle_c \\
&+\nabla_{\mathbf{x}}\langle \overline{h}(\mathbf{x}, \lambda)\rangle_c \nabla_{\mathbf{y}}^T u_c(\mathbf{x}, \mathbf{y}, s)\langle K(\mathbf{y})\rangle_c \\
&+\langle K'(\mathbf{x})K'(\mathbf{y})\rangle_c \nabla_{\mathbf{x}}\langle \overline{h}(\mathbf{x}, \lambda)\rangle_c \nabla_{\mathbf{y}}^T\langle h(\mathbf{y}, s)\rangle_c \\
&+\nabla_{\mathbf{x}}\langle \overline{h}(\mathbf{x}, \lambda)\rangle_c \langle K'(\mathbf{x})K'(\mathbf{y})\nabla_{\mathbf{y}}^T h'(\mathbf{y}, s)\rangle_c \\
&+\left\langle K'(\mathbf{x})\nabla_{\mathbf{x}}\bar{h}'(\mathbf{x}, \lambda)\nabla_{\mathbf{y}}^T h'(\mathbf{y}, s)\right\rangle_c \langle K(\mathbf{y})\rangle_c \\
&+\left\langle K'(\mathbf{x})K'(\mathbf{y})\nabla_{\mathbf{x}}\bar{h}'(\mathbf{x}, \lambda)\right\rangle_c \nabla_{\mathbf{y}}^T\langle h(\mathbf{y}, s)\rangle_c \\
&+\left\langle K'(\mathbf{x})K'(\mathbf{y})\nabla_{\mathbf{x}}\bar{h}'(\mathbf{x}, \lambda)\nabla_{\mathbf{y}}^T h'(\mathbf{y}, s)\right\rangle_c
\end{aligned} \tag{28}
$$

where $\overline{u}_c(\mathbf{y}, \mathbf{x}, \lambda) = \langle K'(\mathbf{y})\bar{h}'(\mathbf{x}, \lambda)\rangle_c$ is given explicitly by (Appendix B)

$$
\begin{aligned}
\overline{u}_c(\mathbf{y}, \mathbf{x}, \lambda) = &-\int_\Omega \overline{\mathbf{r}}_c(\mathbf{z}, \lambda) \cdot \nabla_{\mathbf{z}}\left\langle \overline{G}(\mathbf{z}, \mathbf{x}, \lambda)K'(\mathbf{y})\right\rangle_c d\mathbf{z} \\
&-\int_\Omega \nabla_{\mathbf{z}}^T\langle \overline{h}(\mathbf{z}, \lambda)\rangle_c \left\langle K'(\mathbf{z})\nabla_{\mathbf{z}}\overline{G}(\mathbf{z}, \mathbf{y}, \lambda)K'(\mathbf{y})\right\rangle_c d\mathbf{z}
\end{aligned} \tag{29}
$$

The conditional variance tensor $\mathbf{C}_{\mathbf{q}c}(\mathbf{x}, \mathbf{x}, t, t)$ of flux is obtained through inverse transformation of $\overline{\mathbf{C}}_{\mathbf{q}c}(\mathbf{x}, \mathbf{x}, \lambda, t)$ at time t. The latter is given explicitly by (Appendix B)

$$\begin{aligned}
\overline{\mathbf{C}}_{\mathbf{q}c}(\mathbf{x},\mathbf{x},\lambda,t) &= -\overline{\mathbf{r}}_c(\mathbf{x},\lambda)\mathbf{r}_c^T(\mathbf{x},t) \\
&+ \langle K(\mathbf{x})\rangle_c\langle\nabla\bar{h}'(\mathbf{x},\lambda)\nabla^T h'(\mathbf{x},t)\rangle_c\langle K(\mathbf{x})\rangle_c \\
&- \langle K(\mathbf{x})\rangle_c\overline{\mathbf{r}}_c(\mathbf{x},\lambda)\nabla^T\langle h(\mathbf{x},t)\rangle_c \\
&+ \langle K(\mathbf{x})\rangle_c\langle K'(\mathbf{x})\nabla\bar{h}'(\mathbf{x},\lambda)\nabla^T h'(\mathbf{x},t)\rangle_c \\
&- \nabla\langle\bar{h}(\mathbf{x},\lambda)\rangle_c\mathbf{r}_c^T(\mathbf{x},t)\langle K(\mathbf{x})\rangle_c \\
&+ \nabla\langle\bar{h}(\mathbf{x},\lambda)\rangle_c\langle K'(\mathbf{x})K'(\mathbf{x})\rangle_c\nabla^T\langle h(\mathbf{x},t)\rangle_c \\
&+ \nabla\langle\bar{h}(\mathbf{x},\lambda)\rangle_c\langle K'(\mathbf{x})K'(\mathbf{x})\nabla^T h'(\mathbf{x},t)\rangle_c \\
&+ \langle K'(\mathbf{x})\nabla\bar{h}'(\mathbf{x},\lambda)\nabla^T h'(\mathbf{x},t)\rangle_c\langle K(\mathbf{x})\rangle_c \\
&+ \langle K'(\mathbf{x})K'(\mathbf{x})\nabla\bar{h}'(\mathbf{x},\lambda)\rangle_c\nabla^T\langle h(\mathbf{x},t)\rangle_c \\
&+ \langle K'(\mathbf{x})K'(\mathbf{x})\nabla\bar{h}'(\mathbf{x},\lambda)\nabla^T h'(\mathbf{x},t)\rangle_c
\end{aligned} \tag{30}$$

4. Recursive Nonlocal Conditional Moment Approximations

[17] To render the above conditional moment equations workable, it is necessary to employ a suitable closure approximation. *Tartakovsky and Neuman* [1998a, 1999] developed recursive nonlocal approximations in space-time to leading orders of σ_Y. Elsewhere [*Ye*, 2002], we develop recursive nonlocal approximations to second order in σ_Y in the Laplace domain. As the latter are similar in principle to the former, we present them here without development.

4.1. Recursive Nonlocal Conditional Mean Approximations in the Laplace Domain

[18] The recursive nonlocal conditional mean flow equations are given to zero order in σ_Y by

$$\left\langle\overline{\mathbf{q}}^{(0)}(\mathbf{x},\lambda)\right\rangle_c = -K_G(\mathbf{x})\nabla\left\langle\overline{h}^{(0)}(\mathbf{x},\lambda)\right\rangle_c \qquad \mathbf{x}\in\Omega \tag{31}$$

$$\begin{aligned}
\nabla\cdot\left\langle\overline{\mathbf{q}}^{(0)}(\mathbf{x},\lambda)\right\rangle_c + S_s(\mathbf{x})\lambda\left\langle\overline{h}^{(0)}(\mathbf{x},\lambda)\right\rangle_c &= \langle\overline{f}(\mathbf{x},\lambda)\rangle \\
+ S_s(\mathbf{x})\langle H_0(\mathbf{x})\rangle \qquad \mathbf{x}\in\Omega
\end{aligned} \tag{32}$$

$$\left\langle\overline{h}^{(0)}(\mathbf{x},\lambda)\right\rangle_c = \langle\overline{H}(\mathbf{x},\lambda)\rangle \qquad \mathbf{x}\in\Gamma_D \tag{33}$$

$$-\left\langle\overline{\mathbf{q}}^{(0)}(\mathbf{x},\lambda)\right\rangle_c\cdot\mathbf{n}(\mathbf{x}) = \langle\overline{Q}(\mathbf{x},\lambda)\rangle \qquad \mathbf{x}\in\Gamma_N \tag{34}$$

and to second order by

$$\begin{aligned}
\left\langle\overline{\mathbf{q}}^{(2)}(\mathbf{x},\lambda)\right\rangle_c &= -K_G(\mathbf{x})\left[\nabla\left\langle\overline{h}^{(2)}(\mathbf{x},\lambda)\right\rangle_c + \frac{\sigma_Y^2(\mathbf{x})}{2}\nabla\left\langle\overline{h}^{(0)}(\mathbf{x},\lambda)\right\rangle_c\right] \\
&+ \overline{\mathbf{r}}_c^{(2)}(\mathbf{x},\lambda) \qquad \mathbf{x}\in\Omega
\end{aligned} \tag{35}$$

$$\nabla\cdot\left\langle\overline{\mathbf{q}}^{(2)}(\mathbf{x},\lambda)\right\rangle_c + S_s(\mathbf{x})\lambda\left\langle\overline{h}^{(2)}(\mathbf{x},\lambda)\right\rangle_c = 0 \qquad \mathbf{x}\in\Omega \tag{36}$$

$$\left\langle\overline{h}^{(2)}(\mathbf{x},\lambda)\right\rangle_c = 0 \qquad \mathbf{x}\in\Gamma_D \tag{37}$$

$$-\left\langle\overline{\mathbf{q}}^{(2)}(\mathbf{x},\lambda)\right\rangle_c\cdot\mathbf{n}(\mathbf{x}) = 0 \qquad \mathbf{x}\in\Gamma_N \tag{38}$$

where the superscript designates orders of approximation in σ_Y, $K_G(\mathbf{x}) = \exp\langle Y(\mathbf{x})\rangle_c$ is the conditional geometric mean of $K(\mathbf{x})$, $\sigma_Y^2(\mathbf{x}) = \langle Y'^2(\mathbf{x})\rangle_c$ is the conditional variance of $Y(\mathbf{x})$, and

$$\begin{aligned}
\overline{\mathbf{r}}_c^{(2)}(\mathbf{x},\lambda) &= \int_\Omega \overline{\mathbf{a}}_c^{(2)}(\mathbf{y},\mathbf{x},\lambda)\nabla_{\mathbf{y}}\left\langle\overline{h}^{(0)}(\mathbf{y},\lambda)\right\rangle_c d\mathbf{y} \\
&= \int_\Omega K_G(\mathbf{x})K_G(\mathbf{y})\langle Y'(\mathbf{x})Y'(\mathbf{y})\rangle_c \\
&\quad\times\nabla_{\mathbf{x}}\nabla_{\mathbf{y}}^T\left\langle\overline{G}^{(0)}(\mathbf{y},\mathbf{x},\lambda)\right\rangle_c\nabla_{\mathbf{y}}\left\langle\overline{h}^{(0)}(\mathbf{y},\lambda)\right\rangle_c d\mathbf{y}
\end{aligned} \tag{39}$$

where $\langle\overline{G}^{(0)}(\mathbf{y}, \mathbf{x}, \lambda)\rangle_c$ is the zero-order approximation of the random Green's function and $\langle Y'(\mathbf{x})Y'(\mathbf{y})\rangle_c$ is the conditional covariance of Y between points $\mathbf{x}$ and $\mathbf{y}$. The first-order approximation is governed by a homogeneous equation subject to homogeneous boundary conditions and so it vanishes identically, $\langle h^{(1)}(\mathbf{x}, \lambda)\rangle_c \equiv 0$. We approximate the mean head and flux by their leading terms up to second order as

$$\begin{aligned}
\left\langle\overline{h}(\mathbf{x},\lambda)\right\rangle_c &\approx \left\langle\overline{h}^{(0)}(\mathbf{x},\lambda)\right\rangle_c + \left\langle\overline{h}^{(2)}(\mathbf{x},\lambda)\right\rangle_c \\
\langle\overline{\mathbf{q}}(\mathbf{x},\lambda)\rangle_c &\approx \left\langle\overline{\mathbf{q}}^{(0)}(\mathbf{x},\lambda)\right\rangle_c + \left\langle\overline{\mathbf{q}}^{(2)}(\mathbf{x},\lambda)\right\rangle_c
\end{aligned} \tag{40}$$

4.2. Recursive Nonlocal Conditional Second Moment Approximations in the Laplace Domain

[19] To second order in σ_Y, $\overline{C}_{hc}^{(0)} = \overline{C}_{hc}^{(1)} = 0$, and the second-order approximation of the conditional head covariance $\overline{C}_{hc}^{(2)}(\mathbf{x}, \mathbf{y}, \lambda, s)$ is governed by

$$\begin{aligned}
&-\nabla_{\mathbf{x}}\cdot\left[K_G(\mathbf{x})\nabla_{\mathbf{x}}\overline{C}_{hc}^{(2)}(\mathbf{x},\mathbf{y},\lambda,s) + u_c^{(2)}(\mathbf{x},\mathbf{y},s)\nabla_{\mathbf{x}}\left\langle\overline{h}^{(0)}(\mathbf{x},\lambda)\right\rangle_c\right] \\
&+ S_s(\mathbf{x})\lambda\overline{C}_{hc}^{(2)}(\mathbf{x},\mathbf{y},\lambda,s) = \\
&S_s(\mathbf{x})\int_\Omega S_s(\mathbf{z})C_{H_0}(\mathbf{x},\mathbf{z})\left\langle G^{(0)}(\mathbf{z},\mathbf{y},s)\right\rangle_c d\mathbf{z} \\
&+ \int_0^s\int_\Omega \overline{C}_f(\mathbf{x},\mathbf{z},\lambda,\tau)\left\langle G^{(0)}(\mathbf{z},\mathbf{y},s-\tau)\right\rangle_c d\mathbf{z}d\tau
\end{aligned} \tag{41}$$

$$\begin{aligned}
\overline{C}_{hc}^{(2)}(\mathbf{x},\mathbf{y},\lambda,s) = &-\int_0^s\int_{\Gamma_D}\overline{C}_H(\mathbf{x},\mathbf{z},\lambda,\tau)K_G(\mathbf{z}) \\
&\times\nabla_{\mathbf{z}}\left\langle G^{(0)}(\mathbf{z},\mathbf{y},s-\tau)\right\rangle_c\cdot\mathbf{n}(\mathbf{z})d\mathbf{z}d\tau \qquad \mathbf{x}\in\Gamma_D
\end{aligned} \tag{42}$$

$$\begin{aligned}
&\left[K_G(\mathbf{x})\nabla_{\mathbf{x}}\overline{C}_{hc}^{(2)}(\mathbf{x},\mathbf{y},\lambda,s) + u_c^{(2)}(\mathbf{x},\mathbf{y},s)\nabla_{\mathbf{x}}\left\langle\overline{h}^{(0)}(\mathbf{x},\lambda)\right\rangle_c\right]\cdot\mathbf{n}(\mathbf{x}) \\
&= \int_0^s\int_{\Gamma_N}\overline{C}_Q(\mathbf{x},\mathbf{z},\lambda,\tau)\left\langle G^{(0)}(\mathbf{z},\mathbf{y},s-\tau)\right\rangle_c d\mathbf{z}d\tau \qquad \mathbf{x}\in\Gamma_N
\end{aligned} \tag{43}$$

where C_{H_0}, $\overline{C}_f$, $\overline{C}_H$, and $\overline{C}_Q$ are transformed covariances of the forcing terms H_0, f, H, and Q, respectively:

$$\begin{aligned}
C_{H_0}(\mathbf{x},\mathbf{z}) &= \langle H_0'(\mathbf{x})H_0'(\mathbf{z})\rangle \\
\overline{C}_f(\mathbf{x},\mathbf{z},\lambda,\tau) &= \left\langle\overline{f}'(\mathbf{x},\lambda)f'(\mathbf{z},\tau)\right\rangle \\
\overline{C}_H(\mathbf{x},\mathbf{z},\lambda,\tau) &= \left\langle\overline{H}'(\mathbf{x},\lambda)H'(\mathbf{z},\tau)\right\rangle \\
\overline{C}_Q(\mathbf{x},\mathbf{z},\lambda,\tau) &= \left\langle\overline{Q}'(\mathbf{x},\lambda)Q'(\mathbf{z},\tau)\right\rangle
\end{aligned} \tag{44}$$

For consistency, we assume that all random fluctuations in forcing terms are of order σ_Y. Perturbation expansion of

$\overline{\mathbf{P}}_c(\mathbf{x}, \mathbf{y}, \lambda, s)$ in equation (25) and $u_c(\mathbf{x}, \mathbf{y}, s)$ in equation (26) yields the leading terms

$$\overline{\mathbf{P}}_c^{(0)}(\mathbf{x},\mathbf{y},\lambda,s) = \overline{\mathbf{P}}_c^{(1)}(\mathbf{x},\mathbf{y},\lambda,s) = \overline{\mathbf{P}}_c^{(2)}(\mathbf{x},\mathbf{y},\lambda,s) \equiv 0 \tag{45}$$

$$\begin{aligned} u_c^{(0)}(\mathbf{x},\mathbf{y},s) &= u_c^{(1)}(\mathbf{x},\mathbf{y},s) \equiv 0 \\ u_c^{(2)}(\mathbf{x},\mathbf{y},s) &= -K_G(\mathbf{x}) \int_0^s \int_\Omega K_G(\mathbf{z}) \langle Y'(\mathbf{z}) Y'(\mathbf{x}) \rangle_c \\ &\quad \times \nabla_z \left\langle h^{(0)}(\mathbf{z},\tau) \right\rangle_c \cdot \nabla_z \left\langle G^{(0)}(\mathbf{z},\mathbf{y},s-\tau) \right\rangle_c d\mathbf{z} d\tau \end{aligned} \tag{46}$$

Perturbation of the conditional covariance $\overline{C}_{hc}(\mathbf{x}, \mathbf{x}, \lambda, t)$ yields leading terms

$$\begin{aligned} &\overline{C}_{hc}^{(0)}(\mathbf{x},\mathbf{x},\lambda,t) = \overline{C}_{hc}^{(1)}(\mathbf{x},\mathbf{x},\lambda,t) \equiv 0 \\ &\overline{C}_{hc}^{(2)}(\mathbf{x},\mathbf{x},\lambda,t) = \\ &-\int_\Omega u_c^{(2)}(\mathbf{y},\mathbf{x},t) \nabla_\mathbf{y} \left\langle \overline{h}^{(0)}(\mathbf{y},\lambda) \right\rangle_c \cdot \nabla_\mathbf{y} \left\langle \overline{G}^{(0)}(\mathbf{y},\mathbf{x},\lambda) \right\rangle_c d\mathbf{y} \\ &+ \int_0^t \int_\Omega \int_\Omega \overline{C}_f(\mathbf{y},\mathbf{z},\lambda,\tau) \left\langle G^{(0)}(\mathbf{z},\mathbf{x},t-\tau) \right\rangle_c \left\langle \overline{G}^{(0)}(\mathbf{y},\mathbf{x},\lambda) \right\rangle_c d\mathbf{z} d\mathbf{y} d\tau \\ &+ \int_\Omega \int_\Omega S_s(\mathbf{y}) S_s(\mathbf{z}) C_{H_0}(\mathbf{y},\mathbf{z}) \left\langle G^{(0)}(\mathbf{z},\mathbf{x},t) \right\rangle_c \left\langle \overline{G}^{(0)}(\mathbf{y},\mathbf{x},\lambda) \right\rangle_c d\mathbf{z} d\mathbf{y} \\ &+ \int_0^t \int_{\Gamma_D} \int_{\Gamma_D} \overline{C}_H(\mathbf{y},\mathbf{z},\lambda,\tau) K_G(\mathbf{z}) \nabla_\mathbf{z} \left\langle G^{(0)}(\mathbf{z},\mathbf{x},t-\tau) \right\rangle_c \cdot \mathbf{n}(\mathbf{z}) \\ &\qquad K_G(\mathbf{y}) \nabla_\mathbf{y} \left\langle \overline{G}^{(0)}(\mathbf{y},\mathbf{x},\lambda) \right\rangle_c \cdot \mathbf{n}(\mathbf{y}) d\mathbf{z} d\mathbf{y} d\tau \\ &+ \int_0^t \int_{\Gamma_N} \int_{\Gamma_N} \overline{C}_Q(\mathbf{y},\mathbf{z},\lambda,\tau) \left\langle G^{(0)}(\mathbf{z},\mathbf{x},t-\tau) \right\rangle_c \left\langle \overline{G}^{(0)}(\mathbf{y},\mathbf{x},\lambda) \right\rangle_c \\ &\times d\mathbf{z} d\mathbf{y} d\tau \end{aligned} \tag{47}$$

[20] Perturbation of the conditional cross-covariance tensor of flux $\overline{\mathbf{C}}_{\mathbf{q}c}(\mathbf{x}, \mathbf{y}, \lambda, s)$ yields leading terms

$$\begin{aligned} &\overline{\mathbf{C}}_{\mathbf{q}c}^{(0)}(\mathbf{x},\mathbf{y},\lambda,s) = \overline{\mathbf{C}}_{\mathbf{q}c}^{(1)}(\mathbf{x},\mathbf{y},\lambda,s) \equiv 0 \\ &\overline{\mathbf{C}}_{\mathbf{q}c}^{(2)}(\mathbf{x},\mathbf{y},\lambda,s) = \\ &K_G(\mathbf{x}) K_G(\mathbf{y}) \Big[\nabla_\mathbf{x} \nabla_\mathbf{y}^T \overline{C}_{hc}^{(2)}(\mathbf{x},\mathbf{y},\lambda,s) \\ &+ \langle Y'(\mathbf{x}) Y'(\mathbf{y}) \rangle_c \nabla_\mathbf{x} \left\langle \overline{h}^{(0)}(\mathbf{x},\lambda) \right\rangle_c \nabla_\mathbf{y}^T \left\langle h^{(0)}(\mathbf{y},s) \right\rangle_c \Big] \\ &+ K_G(\mathbf{x}) \nabla_\mathbf{x} \overline{u}_c^{(2)}(\mathbf{y},\mathbf{x},\lambda) \nabla_\mathbf{y}^T \left\langle h^{(0)}(\mathbf{y},s) \right\rangle_c \\ &+ K_G(\mathbf{y}) \nabla_\mathbf{x} \left\langle \overline{h}^{(0)}(\mathbf{x},\lambda) \right\rangle_c \nabla_\mathbf{y}^T u_c^{(2)}(\mathbf{x},\mathbf{y},s) \end{aligned} \tag{48}$$

The leading terms of $\overline{u}_c(\mathbf{y}, \mathbf{x}, \lambda)$ are

$$\begin{aligned} \overline{u}_c^{(2)}(\mathbf{y},\mathbf{x},\lambda) &= -K_G(\mathbf{y}) \int_\Omega K_G(\mathbf{z}) \langle Y'(\mathbf{z}) Y'(\mathbf{y}) \rangle_c \\ &\quad \times \nabla_\mathbf{z}^T \left\langle \overline{h}^{(0)}(\mathbf{z},\lambda) \right\rangle_c \nabla_\mathbf{z} \left\langle \overline{G}^{(0)}(\mathbf{z},\mathbf{x},\lambda) \right\rangle_c d\mathbf{z} \end{aligned} \tag{49}$$

Perturbation of $\overline{\mathbf{C}}_{\mathbf{q}c}(\mathbf{x}, \mathbf{x}, \lambda, t)$ yields

$$\begin{aligned} \overline{\mathbf{C}}_{\mathbf{q}c}^{(0)}(\mathbf{x},\mathbf{x},\lambda,t) &= \overline{\mathbf{C}}_{\mathbf{q}c}^{(1)}(\mathbf{x},\mathbf{x},\lambda,t) \equiv 0 \\ \overline{\mathbf{C}}_{\mathbf{q}c}^{(2)}(\mathbf{x},\mathbf{x},\lambda,t) &= K_G(\mathbf{x}) K_G(\mathbf{x}) \Big[\Big\langle \left[\nabla \overline{h}'(\mathbf{x},\lambda) \nabla^T h'(\mathbf{x},t) \right]^{(2)} \Big\rangle_c \\ &\quad + \sigma_Y^2(\mathbf{x}) \nabla \left\langle \overline{h}^{(0)}(\mathbf{x},\lambda) \right\rangle_c \nabla^T \left\langle h^{(0)}(\mathbf{x},t) \right\rangle_c \Big] \\ &\quad - K_G(\mathbf{x}) \overline{\mathbf{r}}_c^{(2)}(\mathbf{x},\lambda) \nabla^T \left\langle h^{(0)}(\mathbf{x},t) \right\rangle_c \\ &\quad - K_G(\mathbf{x}) \nabla \left\langle h^{(0)}(\mathbf{x},\lambda) \right\rangle_c \overline{\mathbf{r}}_c^{(2)T}(\mathbf{x},t) \end{aligned} \tag{50}$$

where the covariance tensor $\langle \nabla \overline{h}'(\mathbf{x}, \lambda) \nabla^T h'(\mathbf{x}, t)^{(2)} \rangle_c$ of head gradient is given by equation (B8) as

$$\begin{aligned} &\Big\langle \left[\nabla \overline{h}'(\mathbf{x},\lambda) \nabla^T h'(\mathbf{x},t) \right]^{(2)} \Big\rangle_c = \\ &-\int_\Omega \nabla_\mathbf{x} \nabla_\mathbf{y}^T \left\langle \overline{G}^{(0)}(\mathbf{y},\mathbf{x},\lambda) \right\rangle_c \\ &\quad \times \nabla_\mathbf{y} \left\langle \overline{h}^{(0)}(\mathbf{y},\lambda) \right\rangle_c \nabla_\mathbf{x}^T u_c^{(2)}(\mathbf{y},\mathbf{x},t) d\mathbf{y} \\ &+ \int_0^t \int_\Omega \int_\Omega \overline{C}_f(\mathbf{y},\mathbf{z},\lambda,\tau) \nabla_\mathbf{x} \left\langle \overline{G}^{(0)}(\mathbf{y},\mathbf{x},\lambda) \right\rangle_c \\ &\qquad \times \nabla_\mathbf{x}^T \left\langle G^{(0)}(\mathbf{z},\mathbf{x},t-\tau) \right\rangle_c d\mathbf{z} d\mathbf{y} d\tau \\ &+ \int_\Omega \int_\Omega S_s(\mathbf{y}) S_s(\mathbf{z}) C_{H_0}(\mathbf{y},\mathbf{z}) \nabla_\mathbf{x} \left\langle \overline{G}^{(0)}(\mathbf{y},\mathbf{x},\lambda) \right\rangle_c \\ &\qquad \times \nabla_\mathbf{x}^T \left\langle G^{(0)}(\mathbf{z},\mathbf{x},t) \right\rangle_c d\mathbf{z} d\mathbf{y} \\ &+ \int_0^t \int_{\Gamma_D} \int_{\Gamma_D} \overline{C}_H(\mathbf{y},\mathbf{z},\lambda,\tau) \\ &\quad \times \nabla_\mathbf{x} \left[K_G(\mathbf{y}) \nabla_\mathbf{y} \left\langle \overline{G}^{(0)}(\mathbf{y},\mathbf{x},\lambda) \right\rangle_c \cdot \mathbf{n}(\mathbf{y}) \right] \\ &\quad \times \nabla_\mathbf{x}^T \left[K_G(\mathbf{z}) \nabla_\mathbf{z} \left\langle G^{(0)}(\mathbf{z},\mathbf{x},t-\tau) \right\rangle_c \cdot \mathbf{n}(\mathbf{z}) \right] d\mathbf{z} d\mathbf{y} d\tau \\ &+ \int_0^t \int_{\Gamma_N} \int_{\Gamma_N} \overline{C}_Q(\mathbf{y},\mathbf{z},\lambda,\tau) \nabla_\mathbf{x} \left\langle \overline{G}^{(0)}(\mathbf{y},\mathbf{x},\lambda) \right\rangle_c \\ &\qquad \times \nabla_\mathbf{x}^T \left\langle G^{(0)}(\mathbf{z},\mathbf{x},t-\tau) \right\rangle_c d\mathbf{z} d\mathbf{y} d\tau \end{aligned} \tag{51}$$

5. Localization of Conditional Mean Flow Equations

[21] As the transformed residual flux $\overline{\mathbf{r}}_c(\mathbf{x}, \lambda)$ and mean flux $\langle \overline{\mathbf{q}}(\mathbf{x}, \lambda) \rangle_c$ are non-Darcian, the notion of effective hydraulic conductivity loses meaning in the context of flow prediction based on ensemble mean quantities. In some special cases, localization of the mean equation is possible so that the flow becomes approximately Darcian in the mean. Localization is valid when (1) $\nabla \langle \overline{h}(\mathbf{x}, \lambda) \rangle_c$ varies slowly in space (not necessarily in time) wherever $\overline{\mathbf{a}}_c(\mathbf{y}, \mathbf{x}, \lambda)$ is nonzero and (2) $\overline{\mathbf{r}}_c(\mathbf{x}, \lambda)$ does likewise wherever $\overline{\mathbf{d}}_c(\mathbf{y}, \mathbf{x}, \lambda)$ is nonzero. Then equation (19) can be approximated via

$$\overline{\mathbf{r}}_c(\mathbf{x},\lambda) \approx \int_\Omega \overline{\mathbf{a}}_c(\mathbf{y},\mathbf{x},\lambda) d\mathbf{y} \nabla \left\langle \overline{h}(\mathbf{x},\lambda) \right\rangle_c + \int_\Omega \overline{\mathbf{d}}_c(\mathbf{y},\mathbf{x},\lambda) d\mathbf{y}\, \overline{\mathbf{r}}_c(\mathbf{x},\lambda) \tag{52}$$

and if $[\mathbf{I} - \int_\Omega \overline{\mathbf{d}}_c(\mathbf{y}, \mathbf{x}, \lambda)d\mathbf{y}]^{-1}$ exists where $\mathbf{I}$ is the identity tensor, equation (52) can be rewritten in local form as

$$\overline{\mathbf{r}}_c(\mathbf{x}, \lambda) \approx \overline{\mathbf{k}}_c(\mathbf{x}, \lambda)\nabla\langle\overline{h}(\mathbf{x}, \lambda)\rangle_c \tag{53}$$

where

$$\overline{\mathbf{k}}_c(\mathbf{x}, \lambda) = \left[\mathbf{I} - \int_\Omega \overline{\mathbf{d}}_c(\mathbf{y}, \mathbf{x}, \lambda)d\mathbf{y}\right]^{-1} \int_\Omega \overline{\mathbf{a}}_c(\mathbf{y}, \mathbf{x}, \lambda)d\mathbf{y} \tag{54}$$

Substituting equation (53) into (15) yields the conditional mean Darcian expression

$$\langle\overline{\mathbf{q}}(\mathbf{x}, \lambda)\rangle_c \approx -\overline{\mathbf{K}}_{c,app}(\mathbf{x}, \lambda)\nabla\langle\overline{h}(\mathbf{x}, \lambda)\rangle_c \tag{55}$$

where $\overline{\mathbf{K}}_{c,app}(\mathbf{x}, \lambda)$ is a spatially varying conditional apparent hydraulic conductivity tensor in the Laplace domain, given by

$$\overline{\mathbf{K}}_{c,app}(\mathbf{x}, \lambda) = \langle K(\mathbf{x})\rangle_c\mathbf{I} - \overline{\mathbf{k}}_c(\mathbf{x}, \lambda) \tag{56}$$

Equations (52)–(56) are identical to those obtained previously by *Tartakovsky and Neuman* [1998b] upon first developing moment expressions in space-time and then applying the Laplace transform. There is no known way to localize second-moment equations. Hence localization yields no information about predictive uncertainty.

[22] To render localized mean equations workable, one needs to evaluate the apparent hydraulic conductivity either by inverse method against measured values of head and flux or by recursive approximation. The latter approach yields to second-order

$$\overline{\mathbf{K}}^{[2]}_{c,app}(\mathbf{x}, \lambda) = K_G(\mathbf{x})\left[\left(1 + \frac{\sigma^2_Y(\mathbf{x})}{2}\right)\mathbf{I} - \int_\Omega K_G(\mathbf{y})\langle Y'(\mathbf{x})Y'(\mathbf{y})\rangle_c\nabla_\mathbf{x}\nabla^T_\mathbf{y}\left\langle\overline{G}^{(0)}(\mathbf{y}, \mathbf{x}, \lambda)\right\rangle_c d\mathbf{y}\right] \tag{57}$$

which requires computing the zero-order Green's function (not needed for inverse solution).

6. Numerical Approach

[23] We solve the recursive nonlocal moment equations and localized mean flow equations in the Laplace domain using a Galerkin finite element scheme similar to that developed for steady state flow by *Guadagnini and Neuman* [1999b]; details beyond those given here are given by *Ye* [2002]. For purposes of Monte Carlo simulation, we use a standard Galerkin finite element scheme on the same grid to solve the Laplace-transformed stochastic flow equations (8)–(11) for random realizations of hydraulic conductivity. Independent Monte Carlo runs are conducted in parallel on multiple processors. We then invert the results numerically from the Laplace back into the time domain using a parallelized version of an algorithm devised by *Crump* [1976] and *De Hoog et al.* [1982]. The latter uses trapezoidal rule to discretize the Laplace parameter into k = 0, 1, 2,..., $2M + 1$ values $\lambda_k = \lambda_0 + ik\pi/T$ where $\lambda_0 = -\ln(E)/(2T)$, $i = \sqrt{-1}$, T is half a Fourier period, and E is a dimensionless discretization error. Following *Crump* [1976], *Sudicky* [1989], and *Gambolati et al.* [1997], we set $T = 0.8t_{\max}$, where $t_{\max}$ is the simulation period, $E = 10^{-6}$, and $M = 23$ to yield stable results.

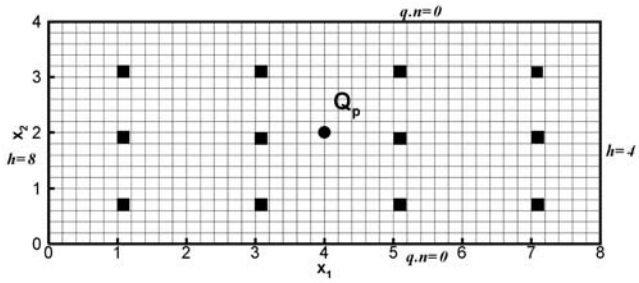

Figure 1. Computational grid, boundary conditions, conditioning points (solid squares) and pumping well (solid circle).

[24] *Sudicky* [1989] and *D'Amore et al.* [1999] have shown that since the algorithm relies on a complex Laplace parameter, it is more accurate than algorithms using real-valued Laplace parameters, which tend to be unstable. Nevertheless, the Gibbs phenomenon may cause the algorithm to yield unstable solutions for $t < 0.1t_{\max}$ (which did not happen in our case). To avoid such instabilities, *Gambolati et al.* [1997] suggested varying $t_{\max}$ so as to ensure that t always remains in the stable range. Another way to eliminate oscillations at relatively small time is to increase M [*Pini and Putti*, 1997].

[25] As finite element moment equations associated with various λ_k values are mutually independent, we solve them in parallel on multiple processors, each of which yields a solution for one or more (depending on the number of processors) λ_k values. Inverse head at any node j in the finite element grid is calculated according to

$$h_j(t) = \frac{1}{T}\exp(\lambda_0 t)\left[\frac{1}{2}h_{j,0} + \sum_{k=1}^{2M+1}\mathrm{Re}\{h_{j,k}\exp(ik\pi t/T)\}\right] \tag{58}$$

where $h_{j,k}$ is the corresponding transformed head at λ_k. Though it is possible to perform these explicit calculations in parallel, our use of a fast quotient-difference algorithm renders it unnecessary.

[26] To compare the accuracy of the three solution methods (recursive nonlocal and localized moment; Monte Carlo) we base all of them on Laplace transformation (according to *Sudicky* [1989] and *Ye* [2002], the latter is more accurate than traditional time marching when applied to a deterministic or single Monte Carlo run). As Monte Carlo simulations are mutually independent we automatically assign each to one processor, which performs the Laplace inversion sequentially for all λ_k values (rather than distributing the inversion among different processors as we do in the case of moment equations). Because of communication between processors [*Mendes and Pereira*, 2003] this results in less than 100% efficiency.

7. Two-Dimensional Examples

[27] We illustrate our approach on conditional and unconditional examples of superimposed mean uniform and convergent flows in a two-dimensional rectangular domain. The domain is subdivided into 800 square elements (20 rows and 40 columns) of uniform size $\Delta x_1 = \Delta x_2 = 0.2$ measured in arbitrary consistent length units (Figure 1). The length of the domain is $L_1 = 40 \times 0.2 = 8$ and its width is $L_2 = 20 \times$

0.2 = 4. A uniform deterministic head $H_L = 8$ (in similar length units) is prescribed on the left boundary ($x_1 = 0$) and a constant head $H_R = 4$ on the right boundary ($x_1 = 8$). The bottom ($x_2 = 0$) and top ($x_2 = 4$) boundaries are impermeable. Constant deterministic initial head $H_0 = 4$ is assigned to all but the prescribed head boundary nodes of the grid. A pumping well (point sink) of deterministic strength Q_p (in arbitrary consistent units of length per time) is placed at the center node of the domain ($x_1 = 4$, $x_2 = 2$). Transient flow is simulated over a period $t_{sim} = 20$ of similar time units. Solutions of the finite element equations are obtained at discrete time steps $t = 0.1, 0.3, 0.5, 0.7, 0.9, 1, 2, 3, 4, 5, 6, 7, 8, 9, 10, 11, 13, 15, 18$, and 20. We employ the same computational grid and time steps for all moment and Monte Carlo solutions to render them directly comparable.

[28] The log hydraulic conductivity $Y(\mathbf{x})$ is taken to be statistically homogeneous and isotropic with the widely used [*Dagan*, 1989; *Zhang*, 2002] exponential covariance function

$$C(r) = \sigma_Y^2 \exp\left(-\frac{r}{l}\right) \tag{59}$$

where r is separation distance (lag) between two points in the domain and l is the integral scale of Y. This choice of covariance function is purely for illustration purposes, our solution algorithms being equally capable of admitting other valid forms of this function. Whereas an exponential covariance causes steady state head variance to grow without limit as the distance between prescribed head boundaries increases, this is not a problem in a finite domain where boundaries render the head statistically nonhomogeneous [*Dagan*, 1989].

[29] For purposes of Monte Carlo simulation we assume that Y is multivariate Gaussian (no such distributional assumption is required for the moment solutions). Random Y fields are generated using the sequential Gaussian simulation code SGSIM [*Deutsch and Journel*, 1998]. Each element is assigned a constant conductivity corresponding to the value generated at its center. We generate 2500 unconditional realizations of Y with mean $\langle Y \rangle = 0$, variance $\sigma_Y^2 = 4$, and correlation scale $l = 1$. The grid thus includes a minimum of five elements per correlation scale as recommended by, among others, *Ababou et al.* [1989].

[30] For purposes of conditional simulation, we "measure" Y (without error) across an unconditional random field at 12 evenly distributed conditioning points shown by solid squares in Figure 1. We then generate 2500 corresponding conditional realizations of Y. Figure 2 depicts images of one such conditional realization and the conditional sample mean m_Y and variance S_Y^2 of all 2500 realizations. As expected, the conditional Y fields are statistically nonhomogeneous in that their mean and variance vary with location.

[31] To render our comparison of nonlocal and localized moment solutions with Monte Carlo results meaningful, the same input statistics (mean, variance, and covariance of Y) are used for all three. We note that for comparative purposes it is not necessary that the Monte Carlo simulations fully stabilize, only that all three sets of input statistics be identical (this was originally pointed out by *Guadagnini and Neuman* [1999a, 1999b]). In practice, nonlocal and localized solutions do not require generating random fields,

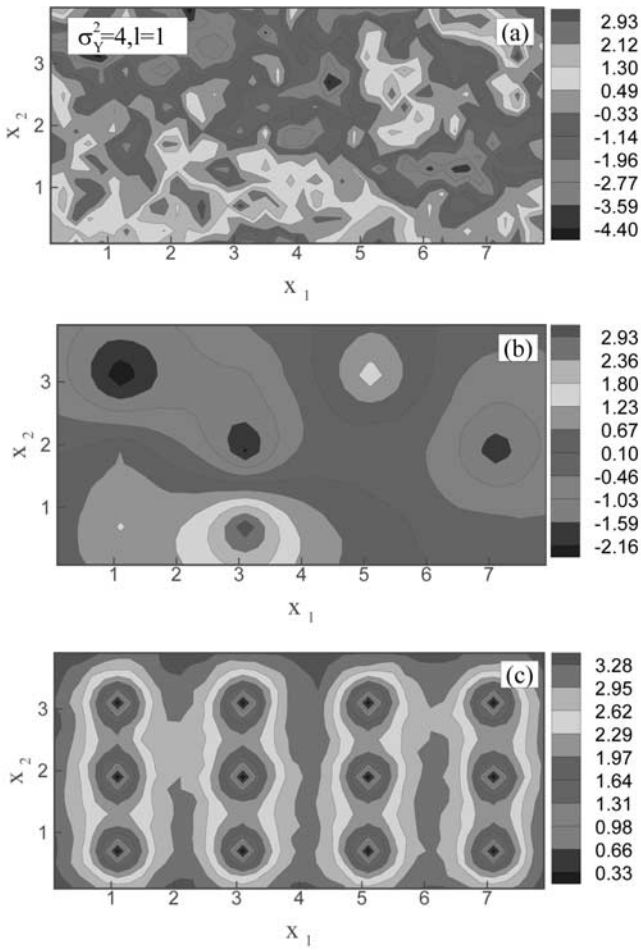

Figure 2. Images of (a) a conditional realization of Y, conditional sample (b) mean m_Y and (c) variance S_Y^2 of $NMC = 2500$ realizations with unconditional $\sigma_Y^2 = 4$, $l = 1$. See color version of this figure at back of this issue.

and one would typically infer the corresponding input statistics from measurements, using geostatistical methods. Upon plotting the sample mean and variance of head and flux at selected points in space-time versus the number of realizations (*Ye* [2002], not shown here), we find that whereas the conditional sample means become effectively stable after about 1000 realizations, the conditional sample variances continue to vary slowly even as the number of realizations approaches our maximum of 2500.

7.1. Conditional Mean Hydraulic Head

[32] Visual examination of conditional mean head contours (*Ye* [2002], not shown here) obtained through recursive nonlocal, localized, and Monte Carlo solutions indicates that the three sets of solutions agree remarkably well. Figure 3 depicts profiles of mean head and second-order mean head corrections at time $t = 5$ along two sections. The localized moment solution is seen to be as accurate (in comparison to the Monte Carlo results) as the nonlocal recursive solution except near the pumping well where it becomes relatively poor due to a steep increase in mean head gradient. The corresponding nonlocal solution is surprisingly accurate considering the strong heterogeneity of the underlying Y field (unconditional $\sigma_Y^2 = 4$). This is

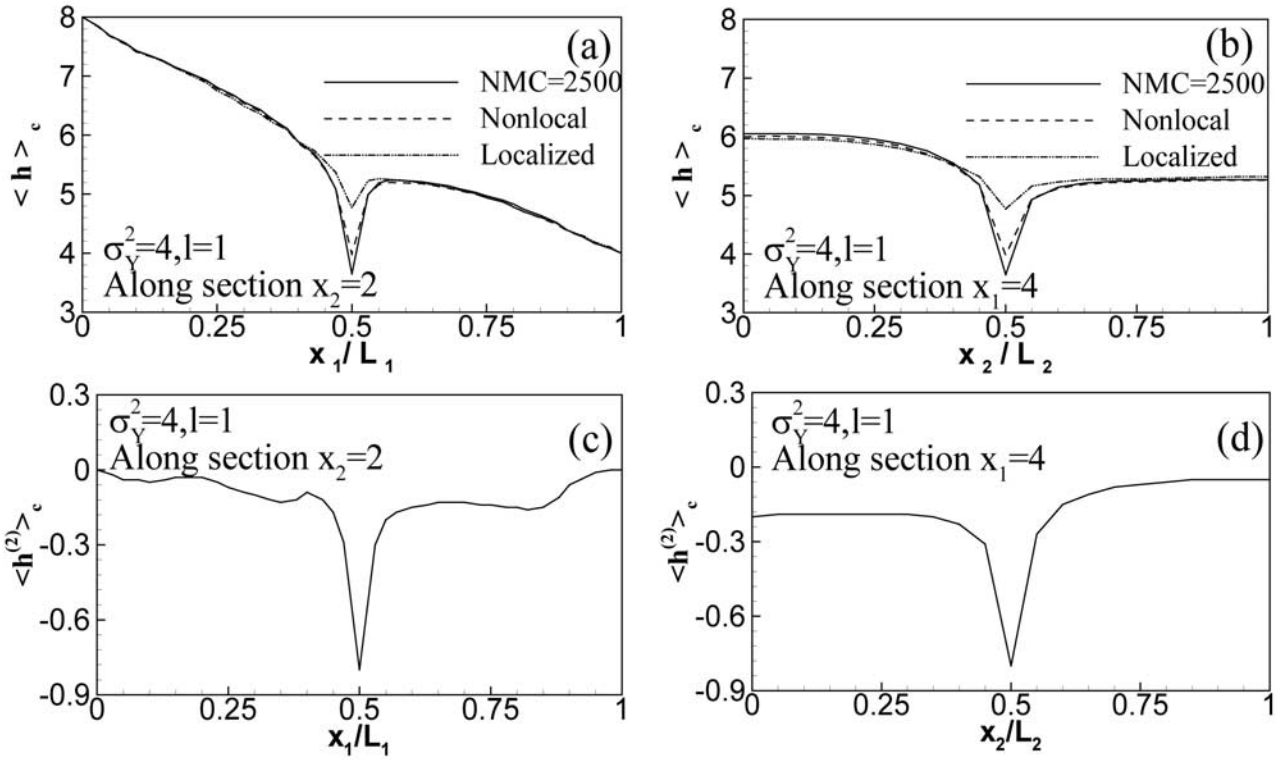

Figure 3. (a and b) Conditional mean head and (c and d) second-order head corrections at time $t = 5$ along longitudinal section $x_2 = 2$ and transverse section $x_1 = 4$ for $\sigma_Y^2 = 4$, $l = 1$.

due to the second-order correction, which is seen to be significant near the well. Results at times other than $t = 5$ (not shown) exhibit similar patterns of behavior.

[33] Figure 4 compares temporal variations in conditional mean head at the pumping well (4.0, 2.0) and at an upstream point (2.0, 2.0) as computed by the three methods of solution (note that the initial head across the domain is 4, as is the head on the left boundary). All three solutions evolve at similar rates at both points. Whereas the nonlocal and localized solutions agree closely with Monte Carlo results at the upstream point, the localized solution seriously overestimates these results at the pumping well. Indeed, the second-order nonlocal correction at the latter is significant at all times. It initially decreases with time and later slowly increases.

7.2. Conditional Variance of Hydraulic Head

[34] Figure 5 compares profiles of conditional head variance at $t = 5$ obtained by the nonlocal (dashed) and Monte Carlo (solid) solution methods. Although our nonlocal results represent the lowest possible order of approximating head variance, they compare remarkably well with MC results except near the pumping well, where they underestimate predictive uncertainty. Elsewhere along the two sections the nonlocal solution overestimates head uncertainty by a small amount. Conditional head variance is zero at the upstream (left) and downstream (right) deterministic Dirichlet boundaries, increasing toward the center of the domain with a sharp rise near the pumping well.

[35] Figure 6 depicts profiles of conditional head variance along section $x_2 = 2$ at times $t = 0.5$, 1, and 10. Profiles after $t = 10$ do not change visibly with time and are therefore not shown. There is good qualitative agreement between the nonlocal and Monte Carlo solutions, which improves quantitatively with time. The manner in which conditional head variance evolves with time at upstream point (2.0, 2.0) and downstream point (6.0, 2.0) is illustrated in Figure 7. Uncertainty is seen to increase and then decrease monotonically with time upstream and increase downstream of the well. There is no qualitative difference between the nonlocal and Monte Carlo results, though they differ quantitatively upstream of the well at early time.

7.3. Conditional Covariance of Hydraulic Head

[36] The covariance is spatially nonhomogeneous due to conditioning and forcing, with acceptable agreement between nonlocal and Monte Carlo results (*Ye* [2002], not shown here). Figure 8 illustrates how the temporal conditional head covariance $C_{hc}(x_1 = y_1 = 2, x_2 = y_2 = 2, t, s)$ varies with time t relative to three reference times $s = 0.5$, 1, and 10. $C_{hc}(\mathbf{x} = \mathbf{y}, t, s)$ is seen to be nonstationary in time due to the transient nature of the problem. For example, $C_{hc}(\mathbf{x} = \mathbf{y}, t = 5, s = 10)$ differs from $C_{hc}(\mathbf{x} = \mathbf{y}, t = 15, s = 10)$ even though both are associated with the same time lag, $|t - s| = 5$. Agreement between the nonlocal and Monte Carlo solutions improves as time and reference time increase.

7.4. Conditional Mean Hydraulic Flux

[37] Figure 9 depicts profiles of longitudinal mean flux, second-order mean flux correction and residual flux at $t = 5$ along two sections. Analogous results for transverse mean flux are shown in Figure 10. Both the nonlocal and localized solutions compare favorably with Monte Carlo simulations, the former more closely than the latter. Second-order components of the longitudinal

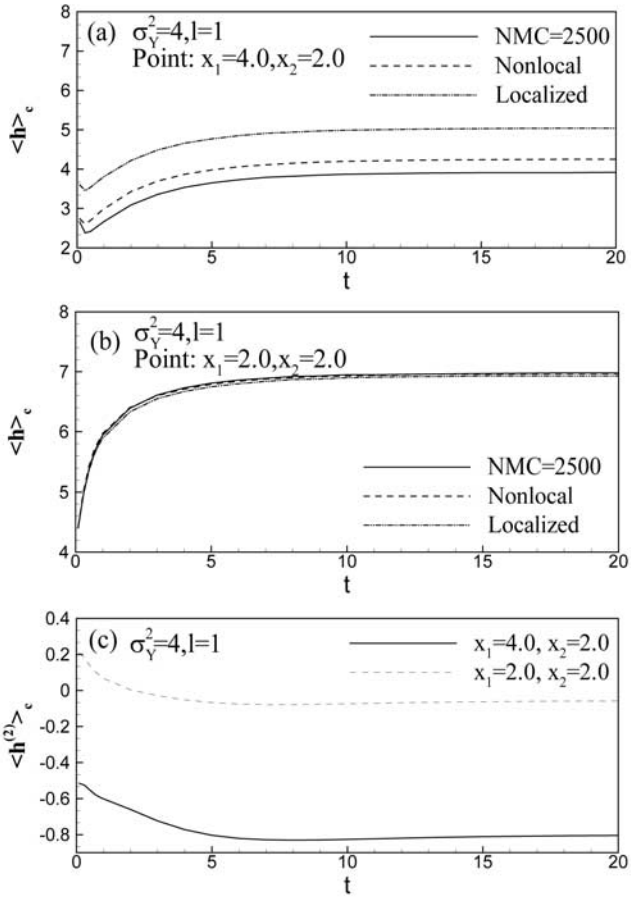

Figure 4. Conditional mean head versus time at points (a) $x_1 = 4$, $x_2 = 2$ (pumping well) and (b) $x_1 = 2.0$, $x_2 = 2.0$ and second-order head corrections at these points for $\sigma_Y^2 = 4$, $l = 1$.

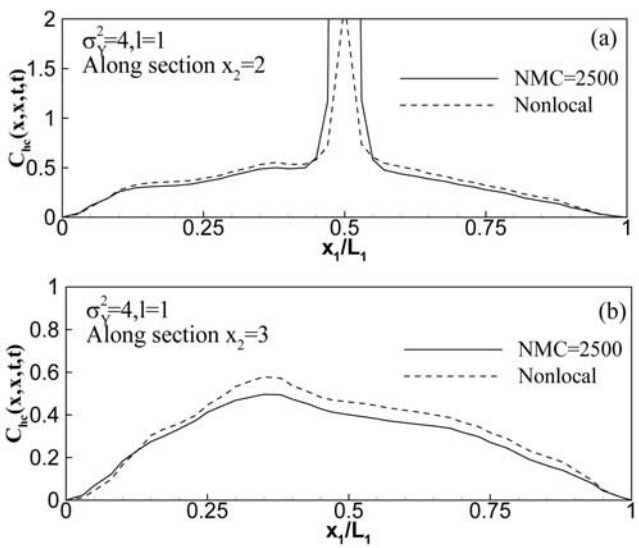

Figure 5. Conditional head variance along sections (a) $x_2 = 2$ and (b) $x_2 = 3$ at time $t = 5$ obtained with $NMC = 2500$ Monte Carlo (solid curves) and nonlocal moment (dashed curves) solutions for $\sigma_Y^2 = 4$, $l = 1$.

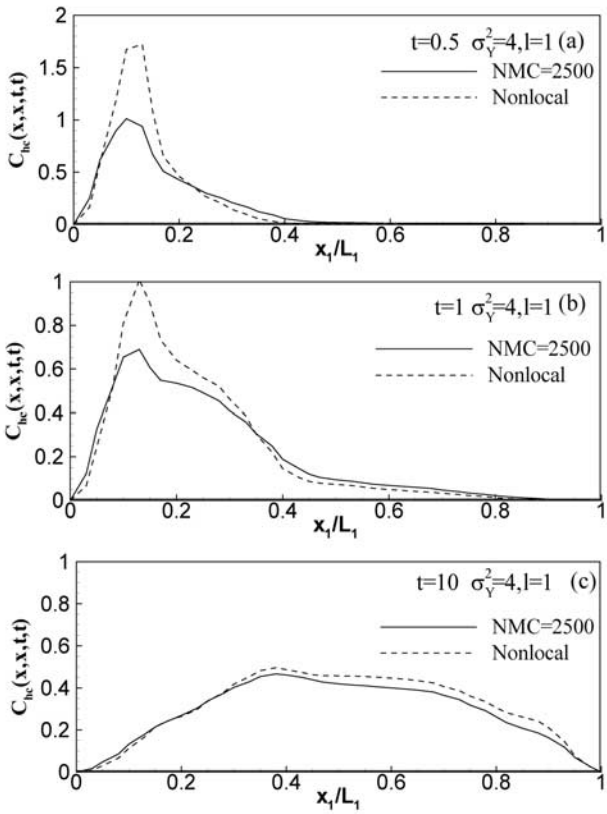

Figure 6. Profiles of conditional head variance along cross sections $x_2 = 3$ at times (a) $t = 0.5$, (b) $t = 1$, and (c) $t = 10$ obtained with $NMC = 2500$ Monte Carlo (solid curves) and nonlocal moment (dashed curves) solutions for $\sigma_Y^2 = 4$, $l = 1$.

mean flux are seen to be strongly affected by the location of conditioning points (open circles in Figures 9e and 9f). Figure 9d indicates that longitudinal mean flux exhibits a maximum at conditioning point (3.1, 0.7) (x_1/L_1 = 0.3875) where mean log conductivity is the largest (Figure 2b), causing mean longitudinal flux to converge. Figure 11 illustrates how conditional longitudinal and

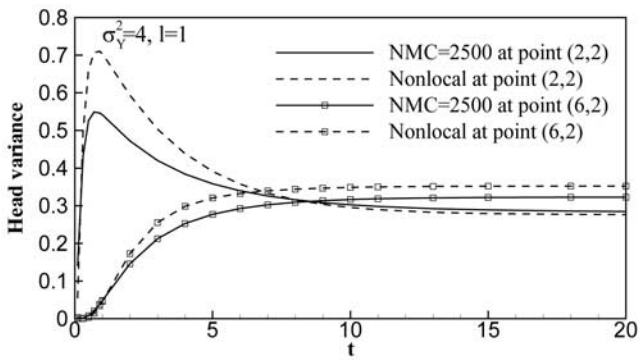

Figure 7. Conditional head variance versus time at points $x_1 = 2$, $x_2 = 2$ (upstream) and $x_1 = 6$, $x_2 = 2$ (downstream) with $NMC = 2500$ Monte Carlo (solid curves) and nonlocal moment (dashed curves) solutions for $\sigma_Y^2 = 4$, $l = 1$.

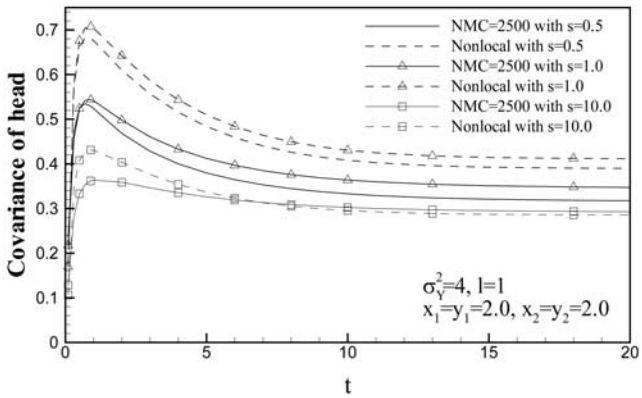

Figure 8. Conditional head covariance for various reference time s = 0.5, 1.0, and 10 at points $x_1 = y_1 = 2.0$, $x_2 = y_2 = 2.0$ obtained with NMC = 2500 Monte Carlo (solid curves) and nonlocal moment (dashed curves) solutions for $\sigma_Y^2 = 4$, $l = 1$.

transverse mean fluxes vary with time at an upstream point.

7.5. Conditional Cross-Covariance Tensor of Flux at Zero Lag

[38] The components of the conditional cross-covariance tensor of flux at zero lag are designated by $C_{qc11}(\mathbf{x}, \mathbf{x}, t, t)$ (longitudinal flux variance), $C_{qc22}(\mathbf{x}, \mathbf{x}, t, t)$ (transverse flux variance), and $C_{qc12}(\mathbf{x}, \mathbf{x}, t, t) = C_{qc21}(\mathbf{x}, \mathbf{x}, t, t)$ (cross-covariance between longitudinal and transverse fluxes). Figures 12–14 depict profiles of these components at time $t = 5$ as computed by the nonlocal and Monte Carlo methods. We note once again that although our nonlocal solution represents the lowest possible order of approximating second moments, these compare remarkably well with the Monte Carlo results, even near the well. Flux variances exhibit maxima in the vicinity of the pumping well. The profile of $C_{qc11}(\mathbf{x}, \mathbf{x}, t, t)$ along section $x_2 = 1.9$ exhibits local minima at conditioning points (open circles in Figure 12a). In Figures 13 and 14, $C_{qc22}(\mathbf{x}, \mathbf{x}, t, t)$ and $C_{qc12}(\mathbf{x}, \mathbf{x}, t, t)$ are close to zero near deterministic boundaries where transverse flux vanishes due to uniform deterministic boundary

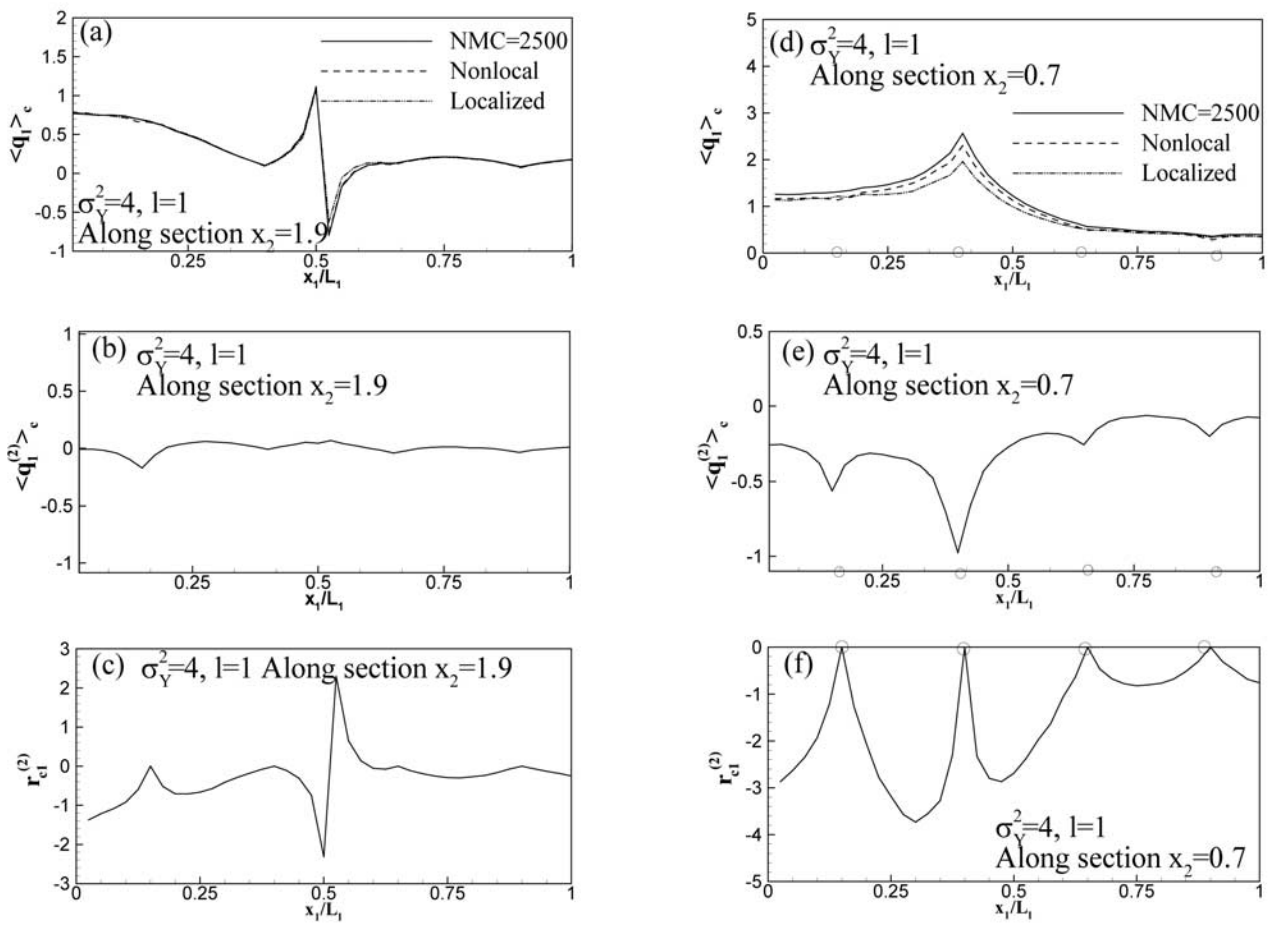

Figure 9. Profiles of conditional longitudinal mean flux, second-order longitudinal mean flux correction and residual flux at time $t = 5$ along sections (a–c) $x_2 = 1.9$ and (d–f) $x_2 = 0.7$ for $\sigma_Y^2 = 4$, $l = 1$. Open circles designate conditioning points.

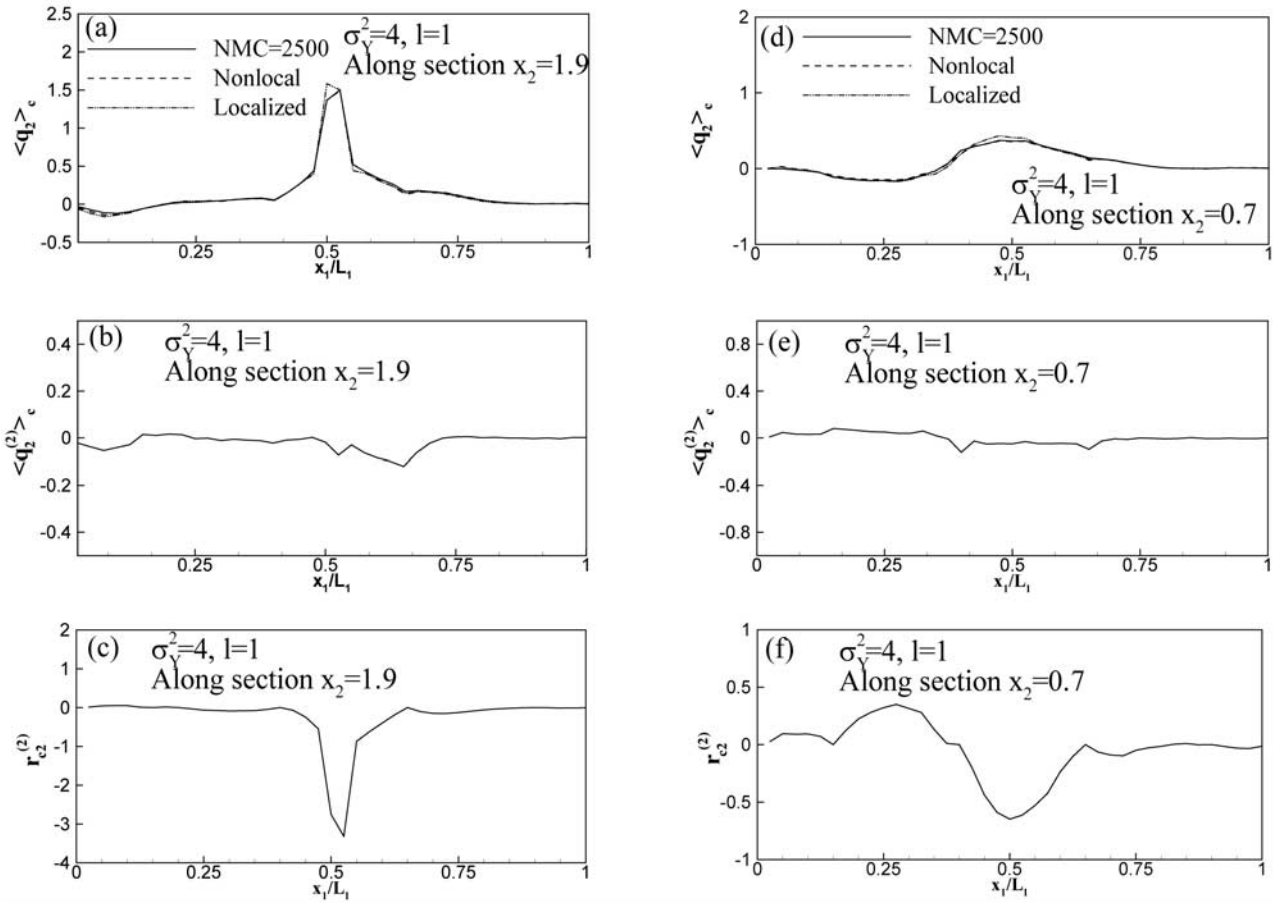

Figure 10. Profiles of conditional transverse mean flux, second-order transverse mean flux correction and residual flux at time $t = 5$ along sections (a–c) $x_2 = 1.9$ and (d–f) $x_2 = 0.7$ for $\sigma_Y^2 = 4$, $l = 1$.

conditions. The profile of $C_{qc12}(\mathbf{x}, \mathbf{x}, t, t)$ is more or less antisymmetric about the pumping well along section $x_2 = 1.9$ (Figure 14a) and uniform along section $x_2 = 2.5$ (Figure 14b).

[39] Figures 15–16 illustrate profiles of $C_{qc11}(\mathbf{x}, \mathbf{x}, t, t)$ and $C_{qc22}(\mathbf{x}, \mathbf{x}, t, t)$ along section $x_2 = 1.9$ at times $t = 0.5$, 1, and 10. Variation with time after $t = 10$ is negligible. Similar profiles of $C_{qc12}(\mathbf{x}, \mathbf{x}, t, t)$ change slightly over time. The nonlocal solution agrees reasonably well with Monte Carlo results, somewhat better at late than at early time. Both $C_{qc11}(\mathbf{x}, \mathbf{x}, t, t)$ and $C_{qc22}(\mathbf{x}, \mathbf{x}, t, t)$ are generally larger upstream than downstream of the pumping well. Figure 17 shows how components of the cross-covariance tensor of flux evolve with time upstream and downstream of the well.

7.6. Comparison of Conditional and Unconditional Moment Solutions

[40] For the sake of brevity, we do not illustrate unconditional solutions corresponding to the above flow problem. Instead, we list in Table 1 the maximum normalized absolute (MNAD) and root mean square (MNRMS) deviations of conditional and unconditional nonlocal moment solutions from corresponding Monte Carlo results, and in Table 2 the maximum and maximum averaged (MA) variances of head and flux as obtained from the conditional and unconditional moment solutions. MNAD and MNRMS are accuracy measures defined as

$$MNAD = \max_{i,j} \left| \frac{P_{i,ME}(t_j) - P_{i,MC}(t_j)}{P_{i,MC}(t_j)} \right|$$
$$MNRMS = \max_{j} \left[\frac{\frac{1}{N}\sum_{i=1}^{N} \left(P_{i,ME}(t_j) - P_{i,MC}(t_j)\right)^2}{\frac{1}{N}\sum_{i=1}^{N} \left(P_{i,MC}(t_j)\right)^2} \right]^{1/2} \quad (60)$$

where $P_{i,ME}(t_j)$ is a moment (mean or variance of head or flux) computed at node i and time t_j using nonlocal moment equations, and $P_{i,MC}(t_j)$ is the same moment computed by Monte Carlo simulation, N being the total number of nodes. The predictive variance measures in Table 2 are maximum $= \max_{i,j} P_{i,ME}(t_j)$ and $MA = \max_{j} \frac{1}{N}\sum_{i=1}^{N} P_{i,ME}(t_j)$ where P now stands for the variance of head or flux.

[41] Table 1 demonstrates that conditioning enhances the overall accuracy of the nonlocal moment solution, as compared to Monte Carlo results. Table 2 shows that conditioning brings about a significant reduction in the maximum and overall predictive variance of head and flux. The latter is seen, for example, upon comparing profiles of

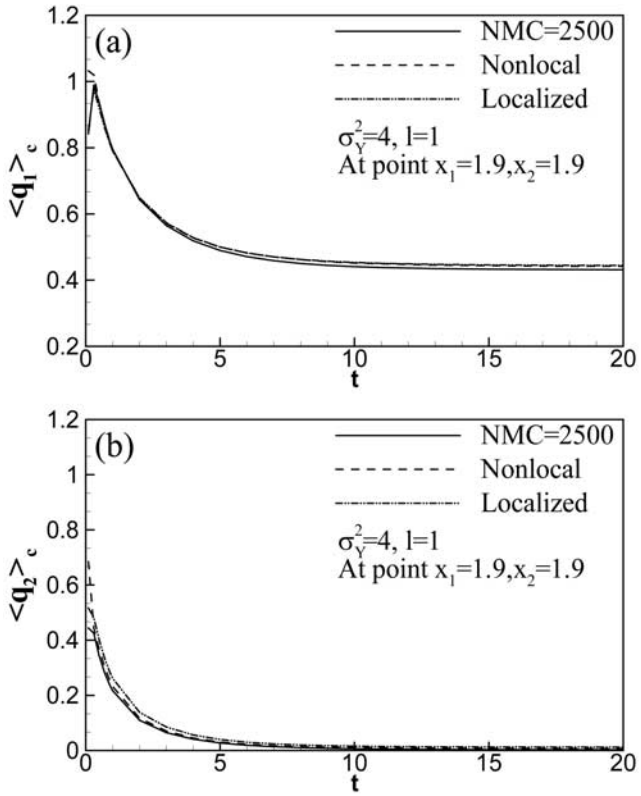

Figure 11. Conditional (a) longitudinal and (b) transverse mean flux versus time at point $x_1 = 1.9$, $x_2 = 1.9$ (upstream) for $\sigma_Y^2 = 4$, $l = 1$.

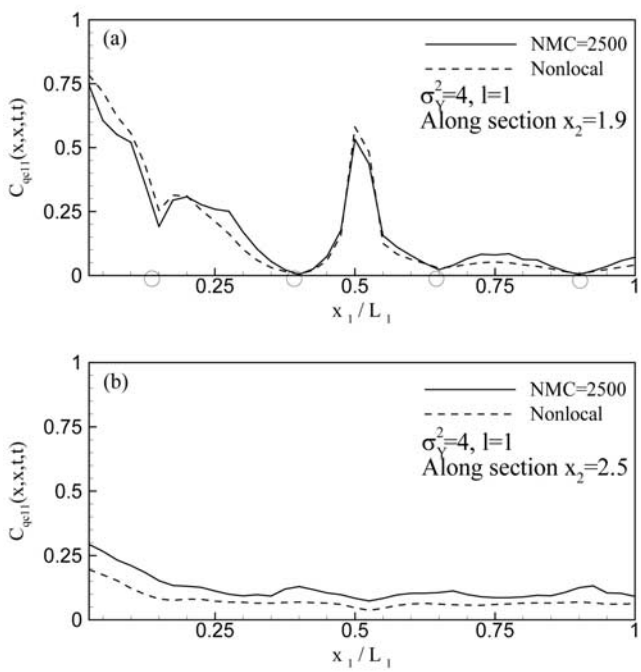

Figure 12. Profiles of conditional variance of longitudinal flux along sections (a) $x_2 = 1.9$ and (b) $x_2 = 2.5$ at time $t = 5$ obtained by *NMC* = 2500 Monte Carlo (solid curves) and nonlocal moment (dashed curves) solutions for $\sigma_Y^2 = 4$, $l = 1$ (conditioning points are marked by circles).

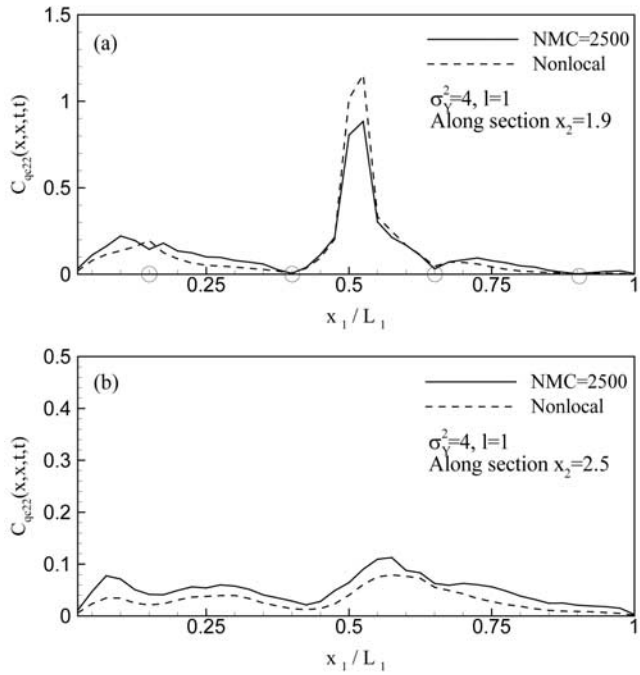

Figure 13. Profiles of conditional variance of transverse flux along sections (a) $x_2 = 1.9$ and (b) $x_2 = 2.5$ at time $t = 5$ obtained with *NMC* = 2500 Monte Carlo (solid curves) and nonlocal moment (dashed curves) solutions for $\sigma_Y^2 = 4$, $l = 1$. Open circles designate conditioning points.

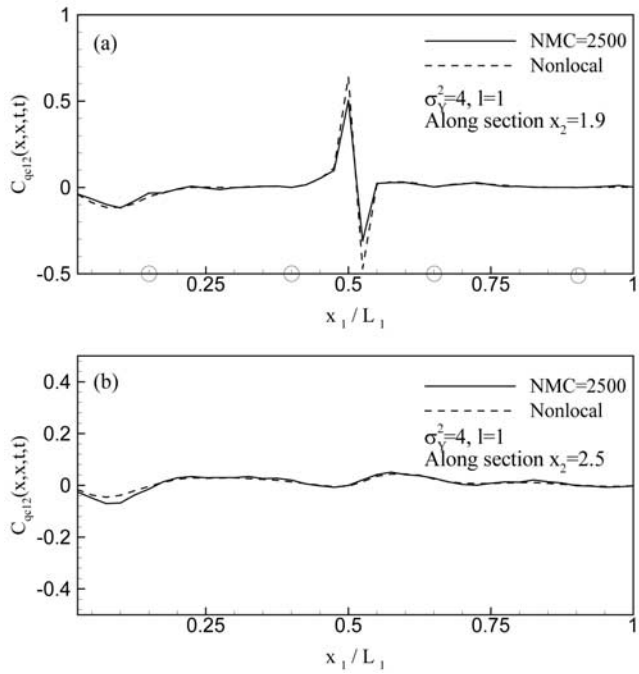

Figure 14. Profiles of conditional cross covariance between longitudinal and transverse flux at zero lag along sections (a) $x_2 = 1.9$ and (b) $x_2 = 2.5$ at time $t = 5$ obtained with *NMC* = 2500 Monte Carlo (solid curves) and nonlocal moment (dashed curves) solutions for $\sigma_Y^2 = 4$, $l = 1$. Open circles designate conditioning points.

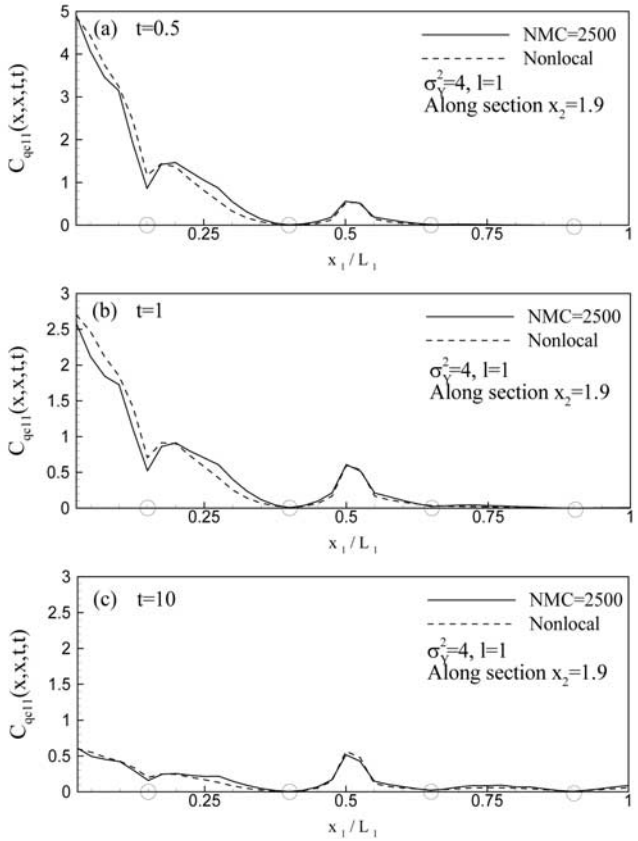

Figure 15. Profiles of conditional variance of longitudinal flux along section $x_2 = 1.9$ at times (a) $t = 0.5$, (b) $t = 1$, and (c) $t = 10$ for $\sigma_Y^2 = 4$, $l = 1$. Open circles designate conditioning points.

unconditional variance of head (Figure 18) and longitudinal flux (Figure 19) at time $t = 5$ with corresponding profiles of conditional variance (Figures 5 and 12, respectively). A comparison of Figures 19 and 12 illustrates the improvement in accuracy achieved through conditioning.

8. Preliminary Comparison of Computational Efficiencies

[42] We compare the computational efficiencies of recursive nonlocal moment and Monte Carlo methods in terms of run times, rather than memory, as (1) optimizing one usually degrades the other and (2) memory is not a major limitation on modern supercomputers, which we use for our examples. In general, the recursive nonlocal method is associated with a larger number of variables (e.g., covariance of log hydraulic conductivity, zero- and second-order head and flux) and therefore requires more memory than does the Monte Carlo method. To ensure that run times are comparable, we use the same computational grid, finite element scheme, and matrix solver for both methods. Parallel computing is done in FORTRAN using message passing interface (MPI), which is portable across a variety of computing platforms, coupled with single program multiple data (SPMD) programming, which allows the same code to run on multiple processors. We recognize that different grid sizes, numerical schemes, matrix solvers, and methods of parallelization may be required to render the run time of each method optimal; as exploring all these possibilities would be outside the scope of this paper, we consider our comparison of computational efficiencies to be of a preliminary nature.

[43] Table 3 compares Monte Carlo (MC) and moment (ME) runtimes required to compute conditional mean and variance of head and flux in the numerical example discussed earlier using one, four, and eight processors on a University of Arizona SGI 2000 supercomputer (recently replaced by a much more powerful HP TRU64 supercomputer). CPU run time is measured by a portable batch system (PBS), which manages jobs submitted to an isolated queue. Our nonlocal moment method consistently outperforms the Monte Carlo method by a significant margin. This is true whether we use one or multiple processors. For example, using one processor to compute conditional mean head takes about 4 times as long with 2500 Monte Carlo runs as with the nonlocal approach; computing conditional head variance takes twice as long. These ratios of run time increase considerably with an increase in the number of processors. The same holds true for the unconditional case.

[44] In addition to grid size, numerical scheme, matrix solver, and method of parallelization, computational efficiency is also influenced by the number of random source terms, number and location of conditioning points, and the number of Monte Carlo runs. In this preliminary comparison we vary the grid size while keeping all other factors

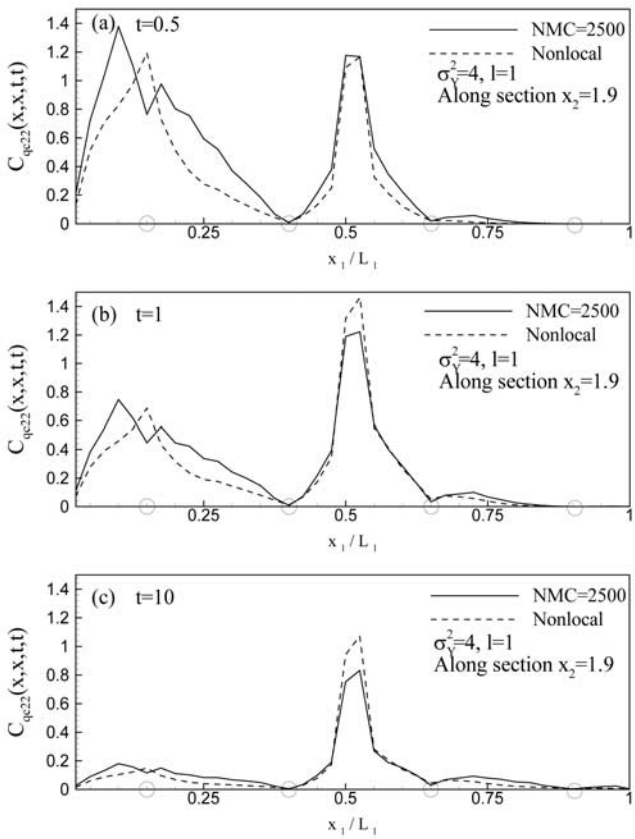

Figure 16. Profiles of conditional variance of transverse flux along section $x_2 = 1.9$ at times (a) $t = 0.5$, (b) $t = 1$, and (c) $t = 10$ for $\sigma_Y^2 = 4$, $l = 1$. Open circles designate conditioning points.

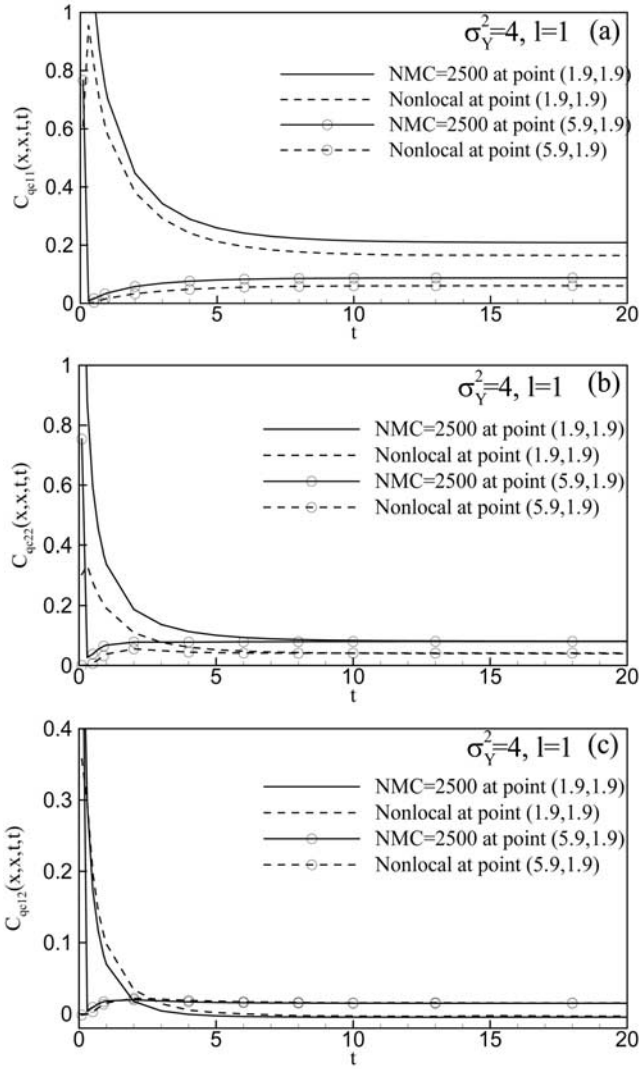

Figure 17. Conditional (a) variance of longitudinal flux, (b) variance of transverse flux, and (c) cross covariance between longitudinal and transverse flux at a zero lag versus time at points $x_1 = 1.9$, $x_2 = 1.9$ (upstream) and $x_1 = 5.9$, $x_2 = 1.9$ (downstream) with *NMC* = 2500 Monte Carlo (solid curves) and nonlocal moment (dashed curves) solutions for $\sigma_Y^2 = 4$, $l = 1$.

Table 1. Maximum Normalized Absolute (MNAD) and Root-Mean-Square (MNRMS) Deviations of Conditional and Unconditional Moment Solutions From Corresponding Monte Carlo Results

	Conditional		Unconditional	
Quantities	MNAD, %	MNRMS, %	MNAD, %	MNRMS, %
Mean head	12.06	0.5762	30.22	1.785
Mean flux q_1	66.67	5.530	86.57	5.709
Mean flux q_2	NA	6.989	NA	12.63
Head variance	87.24	73.50	97.62	93.42
Flux q_1 variance	97.60	28.31	99.63	53.05
Flux q_2 variance	100.0	22.21	100.0	64.63

Table 2. Maximum and Maximum Averaged (MA) Conditional and Unconditional Moment Solutions

	Conditional		Unconditional	
Quantities	Maximum	MA	Maximum	MA
Head variance	2.1584	0.3734	2.9867	0.8749
Flux q_1 variance	2.6436	0.6824	3.0940	0.8834
Flux q_2 variance	0.6763	0.1214	1.8328	0.1354

fixed, without conditioning. In particular, we employ a direct LU factorization method (using the DLSACB, DLFTCB, and DLFSCB routines of the IMSL library on www.vni.com) and 2000 Monte Carlo runs. As full stabilization of all corresponding sample statistics may require many more such runs (e.g., 20,000 in the case of *S. Li et al.* [2003] and 9000 and in the case of *L. Li et al.* [2003]), our comparison is biased in this sense in favor of the Monte Carlo method. It is biased in favor of the nonlocal recursive method in that the latter would entail extra terms for second moments of random sources.

[45] Figure 20a depicts ratios between runtimes required for Monte Carlo and recursive nonlocal computations of mean head and head variance on the University of Arizona HP TRU64 supercomputer using one and 16 processors. Our conditional example runs about 3 times faster on the HP than on the SGI machine. Following optimization of our codes on the HP machine, we find that as grid size increases eightfold from 800 to 6400 finite elements, the run time ratio for mean head decreases by a factor of 7.5 from 68.77 to 9.18 and that for head variance by a factor of 11 from 15.37 to 1.36 with one processor. When 16 processors are used, these ratios drop slightly in a manner that does not appear to have practical significance. The drop is due to a somewhat better parallel performance of the Monte Carlo method in comparison to the nonlocal recursive algorithm, as is seen in Figure 20b; the latter compares the speedups of the Monte Carlo, nonlocal mean head, and nonlocal head

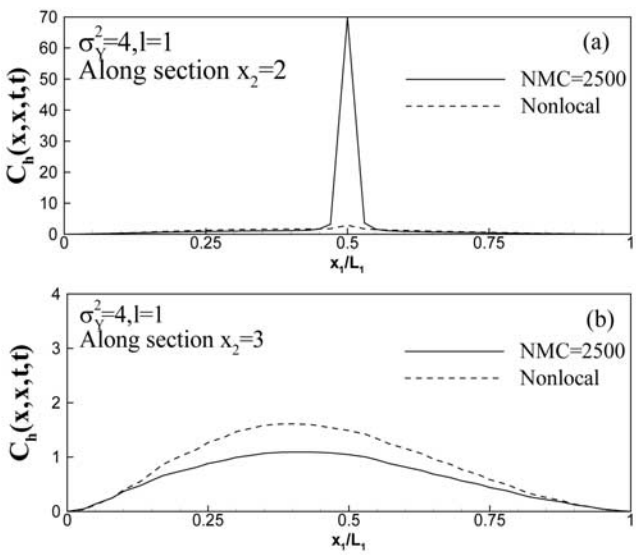

Figure 18. Unconditional head variance along sections (a) $x_2 = 2$ and (b) $x_2 = 3$ at time $t = 5$ obtained with *NMC* = 2500 Monte Carlo (solid curves) and nonlocal moment (dashed curves) solutions for $\sigma_Y^2 = 4$, $l = 1$.

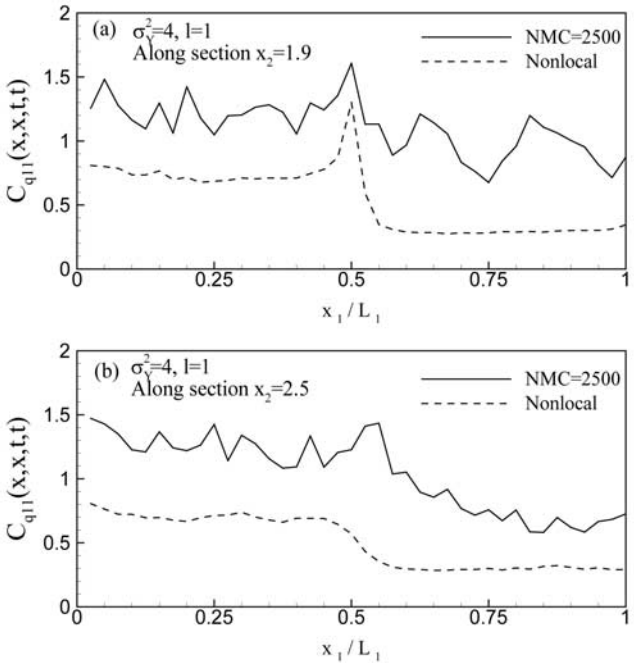

Figure 19. Unconditional variance of longitudinal flux along sections (a) $x_2 = 1.9$ and (b) $x_2 = 2.5$ at time $t = 5$ obtained by $NMC = 2500$ Monte Carlo (solid curves) and nonlocal moment (dashed curves) solutions for $\sigma_Y^2 = 4$, $l = 1$.

variance solutions with number of processors for the largest grid of 6400 elements, a speedup of 1:1 being ideal. It is common for speedup to decrease with the number of processors due to an increase in overhead caused by factors such as system idling and communication between processors. The speedup of nonlocal mean head computation is lower than that of nonlocal variance computation because the former requires solving four coupled moment equations (zero-order head, zero-order Green's function, second-order residual flux, and second-order head) and the latter only three (zero-order head, zero-order Green's function, and second-order head variance).

9. Conclusions

[46] Our work leads to the following major conclusions:

[47] 1. It is possible and computationally feasible to render optimum unbiased predictions of transient groundwater flow, and to assess the corresponding prediction uncertainty in bounded, randomly heterogeneous porous media conditional on measurements without resorting to Monte Carlo simulation. We have done so by solving Laplace-transformed recursive conditional nonlocal moment equations using finite elements and numerical inversion of the results back into the time domain (use of the Laplace transform is limited to linear problems such as ours). Although our theoretical approach allows accounting formally for uncertainty in initial, boundary, and source terms, we have not yet explored this feature of our solution method numerically.

[48] 2. The moment equations we use are distribution-free and thus obviate the need to know or assume the multivariate distributions of random input parameters or forcing terms, as is required for the Monte Carlo approach.

[49] 3. Our approach differs fundamentally from standard perturbative solutions in that it originates in a set of conditional moment equations which are exact, compact, formally incorporate boundary effects, provide a unique insight into the nature of the problem, and lead to unique localized moment equations that look like standard deterministic flow (and transport) equations, allowing one to interpret the latter within a conditional stochastic frame-

Table 3. Run Times, in Minutes, of Monte Carlo (MC) and Nonlocal Moment (ME) Solutions Required to Compute Conditional Mean and Variance of Head and Flux Using P = One, Four, and Eight Processors on the University of Arizona SGI 2000 Supercomputer

		Variables			
		$\langle h \rangle_c$	$\langle \mathbf{q} \rangle_c$	σ_h^2	$\sigma_{\mathbf{q}}^2$
P = 1	MC	831.90	833.58	831.90	833.50
	ME	212.83	212.85	494.30	768.51
P = 4	MC	259.20	260.88	259.20	260.80
	ME	56.59	56.61	135.36	213.25
P = 8	MC	157.80	159.49	157.80	159.40
	ME	33.90	33.92	80.59	121.12

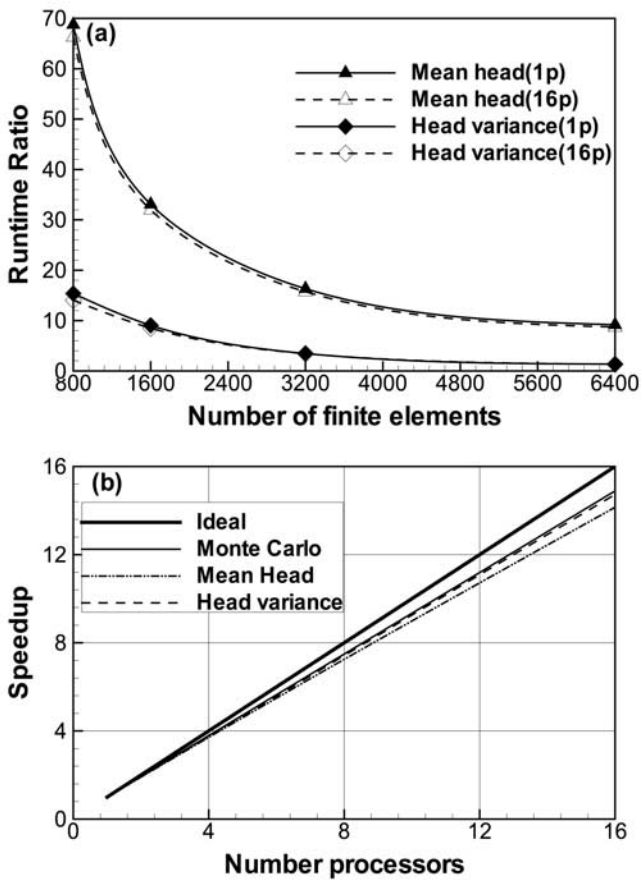

Figure 20. (a) Run time ratio between 2000 Monte Carlo runs and mean head and head variance solutions for different problem sizes using one and 16 processors. (b) Speedup of these solutions for problem of 6400 elements using multiple processors.

work. Both the nonlocal and localized equations describe the space-time evolution of moments representing random functions rendered statistically inhomogeneous (in space) and nonstationary (in time) due to the combined effects of sources, boundaries, and conditioning. To approximate the exact moment equations recursively, we use a valid expansion in terms of (deterministic) moments rather than a theoretically invalid expansion in terms of random quantities, which may (but is not guaranteed to) yield valid results after subsequent averaging. Our approach leads to localized approximations which do not arise from standard perturbation schemes.

[50] 4. Our approach differs computationally from standard perturbative solutions in that it leads to localized moment equations that are almost as easy to solve as standard deterministic flow equations, and to recursive nonlocal moment equations written in terms of Green's functions, which are independent of internal sources and the magnitudes of boundary terms. Once these functions have been computed for a given boundary configuration, they can be used repeatedly to obtain solutions for a wide range of internal sources and boundary terms (scenarios).

[51] 5. Though our localized algorithm is mathematically much simpler and computationally more efficient than the nonlocal algorithm, it has the disadvantage of being less accurate and unable to provide information about predictive uncertainty.

[52] 6. Our nonlocal recursive moment solution cannot be guaranteed to converge for strongly heterogeneous media with log hydraulic conductivity standard deviation, σ_Y, of order 1 or larger. Yet upon submitting it to a severe test by considering superimposed mean uniform and convergent flows in a strongly heterogeneous medium with $\sigma_Y = 4$, the solution proved to be remarkably accurate upon conditioning it on 12 "measured" log conductivity values. Removing the conditioning points caused accuracy to diminish but the solution remained acceptable. Hence the method appears to be applicable to complex flows in strongly heterogeneous media with or without conditioning.

[53] 7. Conditioning was shown to bring about a significant reduction in the predictive uncertainty of head and flux.

[54] 8. A preliminary comparison of supercomputer runtimes for mean head and its variance suggests that our nonlocal moment algorithm consistently outperforms the Monte Carlo method by a significant margin when the same direct matrix solver is used for all three (we do not presently know how using iterative solvers would have affected this conclusion). The ratio between Monte Carlo and nonlocal recursive run times diminishes toward an apparent asymptote as problem size increases, regardless of number of processors.

[55] 9. Our nonlocal algorithm is potentially well suited for groundwater optimization problems and for the investigation of various flow scenarios in randomly heterogeneous aquifers. This is so because the corresponding finite element matrices are independent of internal source terms or the magnitudes of initial and boundary terms. Hence they can be factored once and then used repeatedly to compute the effect of varying the forcing terms on predicted head and flux and on the associated prediction errors. This is in contrast to the Monte Carlo method, which requires repeating all simulations whenever there is a change in forcing terms.

[56] 10. The underlying exact and recursive moment equations, as well as the proposed computational algorithm, are valid in both two and three dimensions, though we have implemented them here in two dimensions.

Appendix A

[57] The random Green's function $\overline{G}(\mathbf{y}, \mathbf{x}, \lambda)$, associated with equations (8)–(11), satisfies

$$-\nabla_{\mathbf{y}} \cdot \left[K(\mathbf{y})\nabla_{\mathbf{y}}\overline{G}(\mathbf{y},\mathbf{x},\lambda)\right] + S_s(\mathbf{y})\lambda\overline{G}(\mathbf{y},\mathbf{x},\lambda) = \delta(\mathbf{y}-\mathbf{x}) \qquad \mathbf{y}\in\Omega \tag{A1}$$

subject to homogeneous boundary conditions

$$\overline{G}(\mathbf{y},\mathbf{x},\lambda) = 0 \qquad \mathbf{y}\in\Gamma_D \tag{A2}$$

$$\nabla_{\mathbf{y}}\overline{G}(\mathbf{y},\mathbf{x},\lambda)\cdot\mathbf{n}(\mathbf{y}) = 0 \qquad \mathbf{y}\in\Gamma_N \tag{A3}$$

where $\delta(\mathbf{y}-\mathbf{x})$ is the Dirac delta function. $\overline{G}(\mathbf{y}, \mathbf{x}, \lambda)$ is symmetric in the Laplace domain. Substituting equations (12)–(14) into (8)–(11), taking conditional ensemble mean, and subtracting the latter from the former yields

$$\begin{aligned}&\nabla\cdot\left[K(\mathbf{x})\nabla\overline{h}'(\mathbf{x},\lambda)\right] + \nabla\cdot\left[K'(\mathbf{x})\nabla\left\langle\overline{h}'(\mathbf{x},\lambda)\right\rangle_c\right]\\ &\quad-\nabla\cdot\left\langle K'(\mathbf{x})\nabla\overline{h}'(\mathbf{x},\lambda)\right\rangle_c - S_s(\mathbf{x})\lambda\overline{h}'(\mathbf{x},\lambda)\\ &\quad= -S_s(\mathbf{x})H_0'(\mathbf{x}) - \overline{f}'(\mathbf{x},\lambda) \qquad \mathbf{x}\in\Omega\end{aligned} \tag{A4}$$

subject to

$$\overline{h}'(\mathbf{x},\lambda) = \overline{H}'(\mathbf{x},\lambda) \qquad \mathbf{x}\in\Gamma_D \tag{A5}$$

$$\begin{aligned}&\left[K(\mathbf{x})\nabla\overline{h}'(\mathbf{x},\lambda) + K'(\mathbf{x})\nabla\left\langle\overline{h}(\mathbf{x},\lambda)\right\rangle_c - \left\langle K'(\mathbf{x})\nabla\overline{h}'(\mathbf{x},\lambda)\right\rangle_c\right]\cdot\mathbf{n}(\mathbf{x})\\ &\quad= \overline{Q}'(\mathbf{x},\lambda) \qquad \mathbf{x}\in\Gamma_N\end{aligned} \tag{A6}$$

Expressing equations (A4)–(A6) in terms of $\mathbf{y}$, multiplying by $\overline{G}(\mathbf{y}, \mathbf{x}, \lambda)$, integrating over Ω, and applying Green's first identity twice gives the desired expression:

$$\begin{aligned}\overline{h}'(\mathbf{x},\lambda) = &\int_\Omega \langle K'(\mathbf{y})\nabla_{\mathbf{y}}\overline{h}'(\mathbf{y},\lambda)\rangle_c\cdot\nabla_{\mathbf{y}}\overline{G}(\mathbf{y},\mathbf{x},\lambda)d\mathbf{y}\\ &-\int_\Omega K'(\mathbf{y})\nabla_{\mathbf{y}}\langle\overline{h}(\mathbf{y},\lambda)\rangle_c\cdot\nabla_{\mathbf{y}}\overline{G}(\mathbf{y},\mathbf{x},\lambda)d\mathbf{y}\\ &+\int_\Omega\overline{f}'(\mathbf{y},\lambda)\overline{G}(\mathbf{y},\mathbf{x},\lambda)d\mathbf{y} + \int_\Omega S_s(\mathbf{y})H_0'(\mathbf{y})\overline{G}(\mathbf{y},\mathbf{x},\lambda)d\mathbf{y}\\ &-\int_{\Gamma_D}\overline{H}'(\mathbf{y},\lambda)K(\mathbf{y})\nabla_{\mathbf{y}}\overline{G}(\mathbf{y},\mathbf{x},\lambda)\cdot\mathbf{n}(\mathbf{y})d\mathbf{y}\\ &+\int_{\Gamma_N}\overline{Q}'(\mathbf{y},\lambda)\overline{G}(\mathbf{y},\mathbf{x},\lambda)d\mathbf{y}\end{aligned} \tag{A7}$$

Applying the operator $K'(\mathbf{x})\nabla$ to equation (A7), taking conditional ensemble mean, and recognizing that driving

forces are statistically uncorrelated with hydraulic conductivity and hence the random Green's function, leads to

$$\begin{aligned}&\left\langle K'(\mathbf{x})\nabla\bar{h}(\mathbf{x},\lambda)\right\rangle_c\\&=\int_\Omega\left\langle K'(\mathbf{x})\nabla_{\mathbf{x}}\nabla_{\mathbf{y}}^T\overline{G}(\mathbf{y},\mathbf{x},\lambda)\right\rangle_c\left\langle K'(\mathbf{y})\nabla\bar{h}'(\mathbf{y},\lambda)\right\rangle_c d\mathbf{y}\\&-\int_\Omega\left\langle K'(\mathbf{x})K'(\mathbf{y})\nabla_{\mathbf{x}}\nabla_{\mathbf{y}}^T\overline{G}(\mathbf{y},\mathbf{x},\lambda)\right\rangle_c\nabla_{\mathbf{y}}\left\langle\bar{h}(\mathbf{y},\lambda)\right\rangle_c d\mathbf{y}\end{aligned}\tag{A8}$$

This coupled with $\bar{\mathbf{r}}_c(\mathbf{x},\ \lambda) = -\langle K'(\mathbf{x})\nabla\bar{h}'(\mathbf{x},\ \lambda)\rangle_c = -\langle K'(\mathbf{x})\nabla\bar{h}(\mathbf{x},\ \lambda)\rangle_c$ leads immediately to equations (19)–(21).

Appendix B

[58] Multiplying equations (A4)–(A6) by $h'(\mathbf{y},\ s)$ and taking conditional ensemble mean gives equations (22)–(24). Expressing equation (B5) of *Tartakovsky and Neuman* [1998a] in terms of $\mathbf{y}$ and s,

$$\begin{aligned}h'(\mathbf{y},s)=&\int_0^s\int_\Omega\langle K'(\mathbf{z})\nabla_{\mathbf{z}}h'(\mathbf{z},\tau)\rangle_c\cdot\nabla_{\mathbf{z}}G(\mathbf{z},\mathbf{y},s-\tau)\,d\mathbf{z}d\tau\\&-\int_0^s\int_\Omega K'(\mathbf{z})\nabla_{\mathbf{z}}\langle h(\mathbf{z},\tau)\rangle_c\cdot\nabla_{\mathbf{z}}G(\mathbf{z},\mathbf{y},s-\tau)d\mathbf{z}d\tau\\&+\int_\Omega S_s(\mathbf{z})H_0'(\mathbf{z})G(\mathbf{z},\mathbf{y},s)d\mathbf{z}\\&+\int_0^s\int_\Omega f'(\mathbf{z},\tau)G(\mathbf{z},\mathbf{y},s-\tau)d\mathbf{z}d\tau\\&-\int_0^s\int_{\Gamma_D}K(\mathbf{z})\nabla_{\mathbf{z}}G(\mathbf{z},\mathbf{y},s-\tau)\cdot\mathbf{n}(\mathbf{z})H'(\mathbf{z},\tau)d\mathbf{z}d\tau\\&+\int_0^s\int_{\Gamma_N}Q'(\mathbf{z},\tau)G(\mathbf{z},\mathbf{y},s-\tau)d\mathbf{z}d\tau\end{aligned}\tag{B1}$$

premultiplying by $K'(\mathbf{x})\nabla_{\mathbf{x}}\bar{h}'(\mathbf{x},\ \lambda)$ and $K'(\mathbf{x})$, and taking conditional ensemble mean leads to the mixed conditional moments (25) and (26), respectively. Multiplying equation (B1) by H_0', $\bar{f}'$, $\bar{H}'$, and $\bar{Q}'$, and taking conditional ensemble mean gives explicit expressions for the mixed conditional moments in equations (22)–(24):

$$\left\langle H_0'(\mathbf{x})h'(\mathbf{y},s)\right\rangle_c=\int_\Omega S_s(\mathbf{z})\left\langle H_0'(\mathbf{x})H_0'(\mathbf{z})\right\rangle\langle G(\mathbf{z},\mathbf{y},s)\rangle_c d\mathbf{z}\tag{B2}$$

$$\left\langle\overline{f}'(\mathbf{x},\lambda)h'(\mathbf{y},s)\right\rangle_c=\int_0^s\int_\Omega\left\langle\overline{f}'(\mathbf{x},\lambda)f'(\mathbf{z},\tau)\right\rangle\langle G(\mathbf{z},\mathbf{y},s-\tau)\rangle_c d\mathbf{z}d\tau\tag{B3}$$

$$\begin{aligned}\left\langle\bar{H}'(\mathbf{x},\lambda)h'(\mathbf{y},s)\right\rangle_c=&-\int_0^s\int_{\Gamma_D}\left\langle\bar{H}'(\mathbf{x},\lambda)H'(\mathbf{z},\tau)\right\rangle\langle K(\mathbf{z})\\&\times\nabla_{\mathbf{y}}G(\mathbf{z},\mathbf{y},s-\tau)\rangle_c\cdot\mathbf{n}(\mathbf{z})d\mathbf{z}d\tau\end{aligned}\tag{B4}$$

$$\begin{aligned}&\left\langle\bar{Q}'(\mathbf{x},\lambda)h'(\mathbf{y},s)\right\rangle_c=\\&\int_0^s\int_{\Gamma_N}\left\langle\bar{Q}'(\mathbf{x},\lambda)Q'(\mathbf{z},\tau)\right\rangle\langle G(\mathbf{z},\mathbf{y},s-\tau)\rangle_c d\mathbf{z}d\tau\end{aligned}\tag{B5}$$

Multiplying equation (A7) by $h'(\mathbf{x},\ t)$ and taking conditional ensemble mean gives equation (27). Substituting equations (12)–(14) into (8) yields

$$\begin{aligned}\overline{\mathbf{q}}'(\mathbf{x},\lambda)=&-\bar{\mathbf{r}}_c(\mathbf{x},\lambda)-\langle K(\mathbf{x})\rangle_c\nabla\overline{h}'(\mathbf{x},\lambda)\\&-K'(\mathbf{x})\nabla\left\langle\overline{h}(\mathbf{x},\lambda)\right\rangle_c-K'(\mathbf{x})\nabla\overline{h}'(\mathbf{x},\lambda)\end{aligned}\tag{B6}$$

Expressing equation (B13) of *Tartakovsky and Neuman* [1998a] in terms of $\mathbf{y}$ and s,

$$\begin{aligned}\mathbf{q}'(\mathbf{y},s)=&-\mathbf{r}_c(\mathbf{y},s)-\langle K(\mathbf{y})\rangle_c\nabla h'(\mathbf{y},s)-K'(\mathbf{y})\nabla\langle h(\mathbf{y},s)\rangle_c\\&-K'(\mathbf{y})\nabla h'(\mathbf{y},s)\end{aligned}\tag{B7}$$

premultiplying the transpose of equation (B7) by (B6), and taking conditional ensemble mean gives equation (28). Multiplying equation (A7) by $K'(\mathbf{y})$ and taking ensemble mean yields equation (29). Applying the operator $\nabla_{\mathbf{x}}$ to equation (A7), postmultiplying by $\nabla_{\mathbf{x}}^T h'(\mathbf{x},\ s)$, and taking conditional ensemble mean leads to

$$\begin{aligned}&\langle\nabla_{\mathbf{x}}\bar{h}'(\mathbf{x},\lambda)\nabla_{\mathbf{x}}^T h'(\mathbf{x},t)\rangle_c=\\&-\int_\Omega\langle\nabla_{\mathbf{x}}\nabla_{\mathbf{y}}^T\overline{G}(\mathbf{y},\mathbf{x},\lambda)\bar{\mathbf{r}}_{\mathbf{c}}(\mathbf{y},\lambda)\nabla_{\mathbf{x}}^T h'(\mathbf{x},t)\rangle_c\,d\mathbf{y}\\&-\int_\Omega\langle K'(\mathbf{y})\nabla_{\mathbf{x}}\nabla_{\mathbf{y}}^T\overline{G}(\mathbf{y},\mathbf{x},\lambda)\nabla_{\mathbf{y}}\langle\bar{h}(\mathbf{y},\lambda)\rangle_c\nabla_{\mathbf{x}}^T h'(\mathbf{x},t)\rangle_c\,d\mathbf{y}\\&+\int_\Omega\langle\bar{f}'(\mathbf{y},\lambda)\nabla_{\mathbf{x}}\overline{G}(\mathbf{y},\mathbf{x},\lambda)\nabla_{\mathbf{x}}^T h'(\mathbf{x},t)\rangle_c\,d\mathbf{y}\\&+\int_\Omega S_s(\mathbf{y})\langle H_0'(\mathbf{y})\nabla_{\mathbf{x}}\overline{G}(\mathbf{y},\mathbf{x},\lambda)\nabla_{\mathbf{x}}^T h'(\mathbf{x},t)\rangle_c\,d\mathbf{y}\\&-\int_{\Gamma_D}\langle K(\mathbf{y})\nabla_{\mathbf{x}}\nabla_{\mathbf{y}}^T\overline{G}(\mathbf{y},\mathbf{x},\lambda)\mathbf{n}(\mathbf{y})\bar{H}'(\mathbf{y},\lambda)\nabla_{\mathbf{x}}^T h'(\mathbf{x},t)\rangle_c\,d\mathbf{y}\\&+\int_{\Gamma_N}\langle\bar{Q}'(\mathbf{y},\lambda)\nabla_{\mathbf{x}}\overline{G}(\mathbf{y},\mathbf{x},\lambda)\nabla_{\mathbf{x}}^T h'(\mathbf{x},t)\rangle_c\,d\mathbf{y}\end{aligned}\tag{B8}$$

[59] **Acknowledgments.** This research was supported by the U.S. Nuclear Regulatory Commission under contract NRC-04-95-038 and by NSF/ITR grant EAR-0110289.

References

Ababou, R., D. McLaughlin, L. W. Gelhar, and A. F. B. Tompson (1989), Numerical simulation of three-dimensional saturated flow in randomly heterogeneous porous media, *Transp. Porous Media*, *4*, 549–565.

Bear, J. (1972), *Dynamics of Fluid in Porous Media*, Dover, Mineola, N. Y.

Carslaw, H. S., and J. C. Jaeger (1959), *Conduction of Heat in Solids*, Oxford Univ. Press, New York.

Crump, K. S. (1976), Numerical inverse of Laplace transform using a Fourier series approximation, *J. Assoc. Comput. Mach.*, *23*(1), 89–96.

Dagan, G. (1982), Analysis of flow through heterogeneous random aquifers: 2. Unsteady flow in confined formations, *Water Resour. Res.*, *18*(5), 1571–1585.

Dagan, G. (1989), *Flow and Transport in Porous Formations*, Springer-Verlag, New York.

D'Amore, L., G. Laccetti, and A. Murli (1999), An implementation of a Fourier series method for the numerical inversion of the Laplace transform, *ACM Trans. Math. Software*, *25*(3), 279–305.

De Hoog, F. R., J. H. Knight, and A. N. Stokes (1982), An improved method for numerical inversion of Laplace transform, *SIAM J. Sci. Stat. Comput.*, *3*(3), 357–366.

Deutsch, C. V., and A. G. Journel (1998), *GSLIB: Geostatistical Software Library and User's Guide*, 2nd ed., Oxford Univ. Press, New York.

Farrell, D. A., A. D. Woodbury, and E. A. Sudicky (1998), Numerical modeling of mass transport in hydrogeologic environments: Performance comparison of the Laplace transform Galerkin and Arnoldi model reduction schemes, *Adv. Water Resour.*, *21*, 217–235.

Gambolati, G., C. Gallo, and C. Paniconi (1997), Comment on "A combined Laplace transform and streamline upwind approach for nonideal transport of solute in porous media" by Linlin Xu and Mark L. Brusseau, *Water Resour. Res.*, *33*(2), 367–368.

Guadagnini, A., and S. P. Neuman (1999a), Nonlocal and localized analyses of conditional mean steady state flow in bounded, randomly nonuniform domains: 1. Theory and computational approach, *Water Resour. Res.*, *35*(10), 2999–3018.

Guadagnini, A., and S. P. Neuman (1999b), Nonlocal and localized analyses of conditional mean steady state flow in bounded randomly nonuniform domains: 2. Computational examples, *Water Resour. Res.*, *35*(10), 3019–3039.

Guadagnini, A., and S. P. Neuman (2001), Recursive conditional moment equations for advective transport in randomly heterogeneous velocity fields, *Transp. Porous Media*, *42*(1/2), 37–67.

Indelman, P. (1996), Average of unsteady flows in heterogeneous media of stationary conductivity, *J. Fluid Mech.*, *310*, 39–60.

Indelman, P. (2000), Unsteady source flow in weakly heterogeneous porous media, *Comput. Geosci.*, *4*, 351–381.

Indelman, P. (2002), On mathematical models of average flow in heterogeneous formations, *Transp. Porous Media*, *48*, 209–224.

Li, L., H. A. Tchelepi, and D. Zhang (2003), Perturbation-based moment equation approach for flow in heterogeneous porous media: Applicability range and analysis of high-order terms, *J. Comput. Phys.*, *188*, 296–317.

Li, S. G., D. McLaughlin, and H. S. Liao (2003), A computational practical method for stochastic groundwater modeling, *Adv. Water Resour.*, *26*, 1137–1148.

Mendes, B., and A. Pereira (2003), Parallel Monte Carlo Driver (PMCD)—A software package for Monte Carlo simulations in parallel, *Comput. Phys. Commun.*, *151*(1), 89–95.

Morgan, M. G., and M. Henrion (1990), *Uncertainty: A Guide to Dealing with Uncertainty in Qualitative Risk and Policy Analysis*, Cambridge Univ. Press, New York.

Naff, R. L., D. F. Haley, and E. A. Sudicky (1998), High-resolution Monte Carlo simulation of flow and conservative transport in heterogeneous porous media: 1. Methodology and flow results, *Water Resour. Res.*, *34*, 663–677.

Neuman, S. P. (1997), Stochastic approach to subsurface flow and transport: A view to the future, in *Subsurface Flow and Transport: A Stochastic Approach*, edited by G. Dagan and S. P. Neuman, pp. 231–241, Cambridge Univ. Press, New York.

Neuman, S. P. (2002), Foreword, in *Stochastic Methods for Flow in Porous Media*, pp. ix–xi, Academic, San Diego, Calif.

Neuman, S. P., and A. Guadagnini (2000), A new look at traditional deterministic flow models and their calibration in the context of randomly heterogeneous media, in *Calibration and Reliability in Groundwater Modelling: Coping With Uncertainty*, edited by F. Stauffer et al., *IAHS Publ.*, *265*, 213–221.

Neuman, S. P., and S. Orr (1993), Prediction of steady state flow in nonuniform geologic media by conditional moments: Exact nonlocal formalism, effective conductivities, and weak approximation, *Water Resour. Res.*, *29*(2), 341–364.

Pini, G., and M. Putti (1997), Parallel finite element Laplace transform method for the nonequilibrium groundwater transport equation, *Int. J. Numer. Methods Eng.*, *40*, 2653–2664.

Shapiro, A., and T. Homem-de-mello (2000), On the rate of convergence of optimal solutions of Monte Carlo approximations of stochastic program, *SIAM J. Control Optim.*, *11*(1), 70–86.

Sudicky, E. A. (1989), The Laplace transform Galerkin technique: A time-continuous finite element theory and application to mass transport in groundwater, *Water Resour. Res.*, *25*(8), 1833–1846.

Tartakovsky, D. M., and S. P. Neuman (1998a), Transient flow in bounded randomly heterogeneous domains: 1. Exact conditional moment equations and recursive approximations, *Water Resour. Res.*, *34*(1), 1–12.

Tartakovsky, D. M., and S. P. Neuman (1998b), Transient flow in bounded randomly heterogeneous domains: 2. Localization of conditional mean equations and temporal nonlocality effects, *Water Resour. Res.*, *34*(1), 13–20.

Tartakovsky, D. M., and S. P. Neuman (1999), Extension of "Transient flow in bounded randomly heterogeneous domains: 1. Exact conditional moment equations and recursive approximations," *Water Resour. Res.*, *35*(6), 1921–1925.

Xu, L., and M. L. Brusseau (1995), A combined Laplace transform and streamline upwind approach for nonideal transport of solute in porous media, *Water Resour. Res.*, *31*(10), 2483–2489.

Ye, M. (2002), Parallel finite element Laplace transform algorithm for transient flow in bounded randomly heterogeneous domains, Ph.D. dissertation, Univ. of Ariz., Tucson.

Zhang, D. (1999), Quantification of uncertainty for fluid flow in heterogeneous petroleum reservoirs, *Physica D*, *133*, 488–497.

Zhang, D. (2002), *Stochastic Methods for Flow in Porous Media*, Academic, San Diego, Calif.

A. Guadagnini, Dipartimento di Ingegneria Idraulica Ambientale e del Rilevamento, Politecnico di Milano, Piazza Leonardo da Vinci 32, 20133 Milan, Italy. (alberto.guadagnini@polimi.it)

S. P. Neuman, Department of Hydrology and Water Resources, University of Arizona, Tucson, AZ 85721, USA. (neuman@hwr.arizona. edu)

D. M. Tartakovsky, Theoretical Division, Group T-7, MS B256, Los Alamos National Laboratory, Los Alamos, NM 87545, USA. (dmt@lanl. gov)

M. Ye, Pacific Northwest National Laboratory, Richland, 620 SW Fifth Avenue, Suite 810, Richland, Portland, OR 97204, USA.

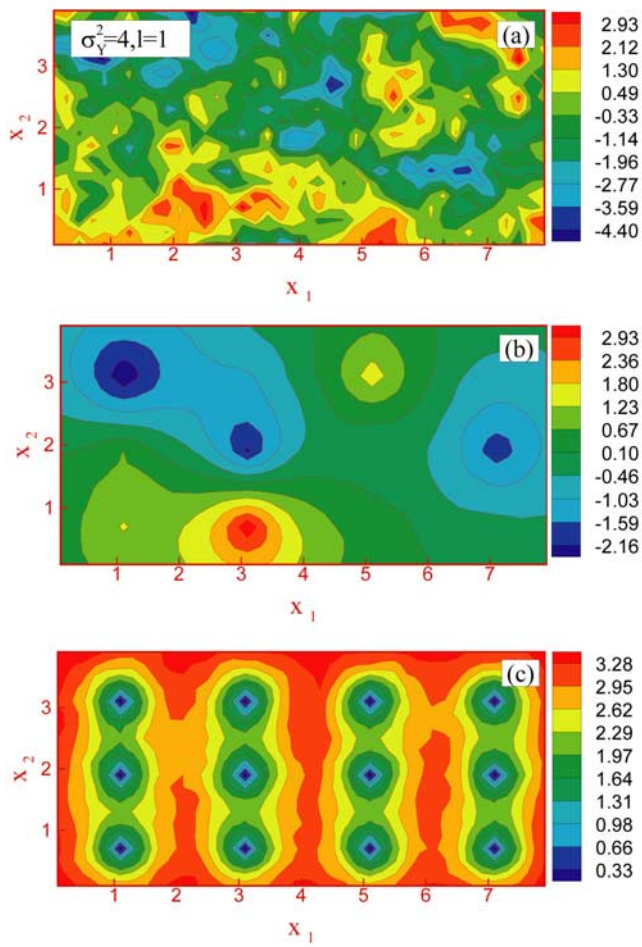

Figure 2. Images of (a) a conditional realization of Y, conditional sample (b) mean m_Y and (c) variance S_Y^2 of $NMC = 2500$ realizations with unconditional $\sigma_Y^2 = 4$, $l = 1$.